INTERNATIONAL ATOMIC ENERGY AGENCY
UNITED NATIONS EDUCATIONAL, SCIENTIFIC AND CULTURAL ORGANIZATION

INTERNATIONAL CENTRE FOR THEORETICAL PHYSICS
34100 TRIESTE (ITALY) - P.O.B. 586 - MIRAMARE - STRADA COSTIERA 11 - TELEPHONE: 2240-1
CABLE: CENTRATOM - TELEX 460392-1

SMR/208 - 22

SPRING COLLEGE IN MATERIALS SCIENCE

ON

"METALLIC MATERIALS"

(11 May - 19 June 1987)

BACKGROUND MATERIAL FOR LECTURES ON "SURFACE TREATMENT AND COATINGS OF MATERIALS"

by

R. BULLOUGH
Materials Development Division
B552 Harwell Laboratory
Oxfordshire OX11 ORA
U.K.

AERE R 12201

AERE R 12201

United Kingdom Atomic Energy Authority

HARWELL

Coatings for gas turbines by sputter ion plating

D S Rickerby* and M I Woods*

*R.A.E. Pyestock,
Farnborough, Hampshire

*Materials Development Division,
Harwell Laboratory, Oxfordshire

April 1986

AERE R 12201

COATINGS FOR GAS TURBINES BY SPUTTER ION PLATING

D S Rickerby+ and M I Woods*

ABSTRACT

This paper reviews the commercially available coating processes used to deposit MCrAlY overlay compositions onto the hot end components of gas turbines. These are compared with sputter ion plating a potentially cheaper and simpler alternative method which has been developed with a view to overcoming some of the limitations shown by the current commercial processes. Particular advantages of sputter ion plating technology include, good control of coating composition, no need to rotate the components to be coated and deposition in a clean environment.

The effect of peening on coating microstructure, and the subsequent oxidation behaviour of the coating, has been examined for a range of MCrAlY compositions. Peening serves to eliminate leader defects from the surface layers by compaction of the coating and also affects the oxide-growth mechanisms. The surface roughness of the SIP coatings, both as-deposited and after glass bead peening, increases with that of the substrate and compares favourably with published values for electron beam evaporated coatings. In addition to protecting the base alloy, coatings must be resistant to thermal fatigue and results are presented for coatings deposited onto UDS superalloys cycled between 1020°C and room temperature using fluidised beds.

*R.A.E., Pyestock, Farnborough, Hampshire.

+Materials Development Division
Harwell Laboratory

April 1986

HL86/1239 (C14)

CONTENTS

TABLES

ILLUSTRATIONS

1. INTRODUCTION

Corrosion has always been one of the most important life limiting factors for the hot end components of marine gas turbines. Even though the early gas turbines used relatively low strength, Cr rich superalloys with a high intrinsic corrosion resistance, it was soon found necessary to coat the components in order to increase their durability. The thrust in gas turbine development over the intervening years towards higher operating temperatures and greater stresses has merely accentuated the problem. To gain strength the general trend of alloy development has been to reduce the Cr content thus lowering the corrosion resistance and further underlining the importance of the coating.

The corrosion resistance of the early coatings, primarily aluminising, has been considerably improved upon with the development of such coatings as Pt-Al and MCrAlY. However, to make best use of the considerable corrosion resistance of such materials it is essential to have a process which is capable of depositing sound coatings of the correct composition. In addition to this exacting requirement, the process must be capable of coating complex shapes whilst simultaneously working within the coating thickness specifications. It must be an adaptable process for it will have to deal with components of widely differing shapes and sizes. Ideally coatings of any composition should be capable of being deposited, but failing this then the ability to handle a wide range of materials would be acceptable. The technique must be reliable, not only in the operation of the equipment but in the standard of the finished product. Finally, the coating system must be cost effective.

Whilst there are already several commercially available coating processes for MCrAlY type materials, e.g. plasma spraying and electron beam evaporation they all have limitations of one kind or another, as does any coating process. For example, plasma sprayed components require time consuming polishing to produce an acceptable surface finish whilst the electron beam evaporation process has difficulty in coping with coating alloys which contain elements with widely differing vapour pressures. Sputter Ion Plating (SIP) has been developed with the

objectives set out above in mind as well as the limitations of the current commercial processes.

2. SPUTTER ION PLATING

SIP[1] is a coating technique which enables one to build up a coating from a flux of atoms and ions which have been sputtered from solid source plates. The equipment (Figure 1) consists of a chamber which is lined with coating source plates and which act as the cathodes for the glow discharge, a mechanical pump for evacuating the unit, a getter and a suitable power supply. The components to be coated are suspended within the volume enclosed by the source plates and are held at a small negative voltage during deposition to control the structure of the coating[2,3]. The coating compartment and its contents are pre-heated to about 300°C to outgas all the exposed surfaces and to enable the establishment of a very pure atmosphere which is important for good coating adhesion. The samples may be cleaned by ion bombardment, if desired, to remove the thin surface oxide layers. A glow discharge is then set up within the chamber by applying a negative voltage of approximately 1000 V to the cathodes. Atoms and ions are sputtered off the cathodes (the coating source plates) and form a flux of material which settles on the components (and exposed parts of the chamber) to form the coating. The relatively small bias voltage on the components (0-100 V) results in "ion polishing" of the coating surface to promote a dense structure without any significant resputtering.

SIP is therefore a very simple technique to operate. Not only is it easy to establish the clean atmosphere required for coating with only a mechanical pump and a getter, but no manipulation of the components is required inside the vacuum system. This latter feature is advantageous not only because it avoids the necessity for complicated handling devices but because it also eliminates the need for constant maintenance of such devices. In addition, since SIP is a batch process, no complex vacuum interlocks, pumping systems and control devices are required.

Sputtering has some distinct advantages over evaporation for the production of alloy coatings. Since the vapour pressures of differing metals can vary by several orders of magnitude at a given temperature,

the flux of atoms being evaporated from an alloy source will have a very different composition to the pool source[4,5]. This difference is carried over into the deposited coating. In addition to this difference in composition, the flux of evaporating species is not necessarily uniform above the molten source pool[4] whereas the coatings deposited by SIP are compositionally uniform throughout the chamber. In order to deposit alloys of a specific composition it is therefore necessary to determine empirical methods of adjusting the composition of the source and to continually monitor the coating composition. Further, because of the difference in composition between the vapour and the molten source pool, any change in the condition of the pool, for example, as a result of a change in power input, temperature distribution or metal feed rate, will alter the composition of the vapour cloud and hence the coating. It takes time to re-establish the former equilibrium. To avoid this requires sophisticated controls on the process, increasing its complexity and need for constant maintenance. For SIP, although different elements do have different sputtering co-efficients, since significant bulk diffusion cannot occur within the source material if the temperature is reasonably low then the loss from the surface of the source plates of the more easily sputtered species cannot be replenished. The surface concentration of these species will only rise once the layers of atoms with lower sputtering coefficients have been removed so as to reveal another layer of atoms, whose average composition will be that of the bulk material, to be sputtered. Hence providing that the source plates are reasonably homogeneous then the flux of coating atoms and ions will be of the same composition as the bulk source plates. Another advantage of SIP is that it has superior throwing power to the evaporation route both because of the distribution of the source material around the components but also because of the randomising effect of the low pressure gas (0.75-1.5 Pa) in the chamber.

Efforts have been made to compare the costs of SIP with some of the techniques currently employed for applying MCrAlY type overlay coatings to turbine blades. The principle commercial techniques are electron beam evaporation and low pressure (or argon shrouded) plasma spraying and the costs are roughly similar for large throughputs. The costs of production using SIP have been shown to compare favourably with these

values. However the costs of electron beam evaporation (in particular) escalate rapidly if the throughput is reduced, whereas the batch production used in SIP results in an almost constant item cost whatever the throughput.

3. RESULTS AND DISCUSSION

3.1 Effect of Peening on Microstructure

Figure 2 shows a CoCrAlY coating on the pressure surface of a Nimonic* turbine blade as coated, and after periods of 114, 500 and 1006 hours at 1000°C. The blade was removed from the furnace once every 24 hours, and cooled to near room temperature before being reinserted. Cycling to low temperature was also carried out on an hourly basis with similar, though slightly accelerated, effects. It is clear from this series of micrographs that aluminium diffuses into the substrate from the inner part of the coating to form NiAl-like fingers and to the surface from the outer part of the coating to form and replenish the protective alumina scale. Figure 3 shows the variation in the Ni, Al, Co and Cr concentrations along a line from outside the oxide scale (left-hand side), through the coating and well into the substrate (right-hand side) for a CoCrAlY coating after 1006 hours at 1000°C; the traces were obtained using an electron probe microanalyser (EPMA). Although the CoAl phase has largely been consumed by this stage, Al is still at about 4 $^{w}/_{o}$ throughout the coating, and this level does not decrease until all the CoAl has disappeared.

All the coatings used to produce the micrographs above were glass bead peened at about 8.5 N before oxidation. A large number of coatings have been tested without peening. In general, the oxidation resistance of unpeened coatings was inferior to the peened equivalents with a tendency to inter-dendritic attack as described by Shaffer et al[6] (particularly at the highest test temperatures). The primary benefits of glass bead peening can be summarised as the generation of an even compressive stress pattern in the surface layers and the elimination of

Throughout the paper * is a registered trademark.

leader defects from, and densification of, the coating. However, peening also hardens the near-surface zone of alloy coatings as shown in Figure 4 for a CoCrAlY coating about 150 μm thick deposited onto a IN792* corrosion pin: similar data has also been obtained for high aluminium NiCrAlTi and Fecralloy steel* coatings. During the initial stages of oxidation the large number of dislocations which formed as a result of the localised hardening induced by the peening operation facilitate the rapid diffusion of aluminium to the surface to form a protective oxide. A comparison of oxides formed on MCrAlY coatings show interesting differences between peened and unpeened samples. For example, Figure 5 shows secondary electron images of the oxides formed on a CoCrAlY coating after 6.5 h at 1000°C. The oxide on the peened surface consists of sharp needle-like growths compared to the rounded morphology of the oxide on the unpeened surface. The gradual loss of the β-CoAl phase from the outermost part of the coating on oxidation is illustrated in Figure 6 which compares diffraction patterns from as-coated material (Figure 6(a)) and coatings with and without peening after oxidation for 6.5 h at 1000°C (Figure 6(b) and (c) respectively). In the early stages of oxidation the predominant peaks appearing on the unpeened surface are characteristic of α-Al_2O_3. However, on the peened surface whilst there is some α-Al_2O_3 there are larger peaks which are within the range of lattice spacings covered by the transition aluminas[7,8]; in each case there are also small peaks which are probably due to spinel oxides. The extra diffraction peaks, and modified oxide structure, remain apparent after 100 h at 1000°C. Figure 7(a) shows a secondary electron image of the oxide scale formed on the peened CoCrAlY coating after oxidation for 100 h at 1000°C, in which both forms of alumina are present. A continuous layer of alpha alumina has formed next to the coating whilst the transitional alumina lies on top of the alpha alumina layer. Similar observations of transitional alumina formation in Fecralloy steels has been reported by Moseley et al[9].

3.2 Effect of Substrate Composition/Surface Roughness on SIP Coatings

A wide variety of alloys are used for the manufacture of rotor blades for gas turbines. To investigate any possible substrate composition effects a set of corrosion pins of different materials

(Nimonic 108*, Mar-M002*, IN738*, IN792* and IN100*) were prepared to the same surface finish (0.16-0.3 μm) and coated by SIP. Figure 8 shows four micrographs of a CoCrAlY coating on a Mar-M002 corrosion pin, and compares the structure of an as-deposited coating (Figure 8(a) and (c)) with that of a glass bead peened coating (Figure 8(b) and (d)) before and after oxidation at 1100°C for 24 h. These micrographs are typical of those observed from all the various alloys coated and show the as-deposited coating to be a finely dispersed two-phase structure (β-CoAl and Co-Cr solid solution for CoCrAlY alloys) with small leader defects present at the near surface of the coating. These leaders are clearly closed by the peening operation. During oxidation at 1100°C the columnar nature of the coating breaks down and the aluminium rich β-CoAl phase is consumed to form a perfectly uniform depleted band at the surface by alumina scale formation. No evidence of oxidation down columnar boundaries is evident in the peened structure (Figure 8(d)), although there is a suggestion of such attack in the as-deposited coating (Figure 8(b)).

From these results it was concluded that substrate composition had no effect on the structure of SIP coatings at a given surface roughness. However, there were differences in the extent of interaction between the various alloys and the CoCrAlY coating when exposed to high temperature oxidation. Figure 9 shows four micrographs of an CoCrAlY coating on an IN738 corrosion pin treated as in Figure 8. There is extensive nickel aluminide formation within the substrate for the Mar-M002 compared with that observed in IN738: in both alloys the β-CoAl phase is gradually consumed from a band near the substrate/coating interface. The varying degrees of nickel alumide formation within the alloys can be related to changes in alloy chemistry resulting from interdiffusion and the stability of the phases formed.

In production it is likely that the surface finish of turbine hardware presented for coating would vary depending on the manufacturing route. The effect of such variations on the surface finish of subsequent SIP coatings is shown in Figure 10 for CoCrAlY coatings deposited onto IN792 corrosion pins of varying surface roughness. The surface roughness of the coatings, both as-deposited and after glass bead peening, is seen to increase with that of the substrate. These

values for SIP coated corrosion pins compare favourably with those given in the literature for electron beam evaporated coatings. Typically for the electron beam process, after surface cleaning, the surface finish of the blades is 1.43 μm which increases slightly to 1.52 μm after coating, falling to 1.30 μm after glass bead peening[10].

Figure 11 shows four micrographs from an CoCrAlY coating on a IN792 corrosion pin which had a surface finish of ~ 3 μm before coating. The as-coated microstructure (Figure 10(a)) shows coarse intercolumnar regions which extend in some cases to the substrate/coating interface: these more open boundaries are associated with the most severe of the surface irregularities. As discussed above, peening services to close up even the most severe of these intercolumnar regions with the result that after oxidation at 1100°C for 24 h oxide penetration down these easy diffusion paths is eliminated[6,11]. The absence of "oxide fingers" in the oxidised coatings after peening is clearly seen in Figure 12, which compares secondary electron images of metallographic sections which have been deep etched in 10% bromine in methanol. For the unpeened coating (Figure 12(a)) oxides have penetrated down to the substrate/coating interface, while peening results in a tight, adherent protective oxide film restricted to the surface of the coating (see Figure 12(b)). SIP coatings deposited onto substrates of a surface roughness of ~ 3 μm will therefore give satisfactory oxidation behaviour provided peening of the coating is carried out to ensure complete closure of leader defects.

3.3 Oxidation and Thermal Shock Tests

Previous sections of this paper have described experiments on CoCrAlY coatings of varying compositions. However, oxidation and corrosion tests have also been carried out on many other coating compositions including NiCrAlY, CoNiCrAlY and NiCrAlTi (compositions are listed in Table 1). Additions of Hf, Zr or Y to several of these materials have also been investigated.

The performance of these coatings has been evaluated in a number of different ways. As with all evaluations, care must be taken in discriminating between the effect on performance of coating integrity,

which may be composition dependent, and the coating chemistry so far as it affects the oxidation/corrosion reactions at the surface. For example, it is generally taken that it is more difficult to deposit CoCrAlY type materials free from leader and flake defects than is the case for NiCrAlY coatings. All else being equal, this must reflect differences in the processes occurring during coating formation as well as the differing responses of the two types of coating materials to post deposition processing such as peening and heat treatment. The response of such a coating, containing as it does some form of structural imperfecton, to a corrosive or oxidising environment will depend upon the severity and form of the test.

When the test is not severe enough to reveal any structural failings of the peened coatings, as seems to be the case with the cyclic oxidation tests, then the effect of differences in composition can be seen. For example, Figure 13 shows a set of micrographs of a NiCrAlTi coating cyclically oxidised at 850°C, a temperature more immediately relevent to marine gas turbines than 1000°C. As can be seen, the coating has been progressively oxidised in a controlled manner when compared with the CoCrAlY coatings presented earlier which established protective oxide scales. However, when the test is more severe, as is the case of thermal shock, then processing differences can become important highlighting any shortcomings in the mechanical integrity of the coatings. Thermal shock tests have been carried out using fluidised hot and cold beds on 100 μm thick CoCrAlY coatings on directionally solidified IN738LC* substrates (test details are in Table 2). The test piece was in the form of a mock aerofoil with an edge radius similar to that for turbine aerofoils. The heat transfer coefficient is likewise comparable with that found for turbine components.

If the coating was heat treated (2 h @ 1120°C) and then peened (8.5 N), cracks initiated within 100-150 cycles. By 300 cycles there was profuse cracking with surface crack lengths of up to 1 mm. In contrast, if the coating process cycle was reversed (peen then heat treat) cracks did not start to form until approximately 800 cycles had elapsed despite obvious plastic deformation of the coating (since the thermal shock specimen was examined in a SEM it was possible to detect crack initiation at a very early stage, corresponding to a surface crack

length of 10-30 μm). Whilst more cracks initiated with further cycling their rate of growth was slower than in the previous case.

A longitudinal section along the trailing edge after 1200 cycles shows the coating originated crack propagating into the substrate (see Figure 14(a)). However, the structure of the adjacent coating shows no tendency towards cracking or internal attack (Figure 14(b)). Similarly there has been no preferential oxidation attack at the substrate-coating interface, which is indicative of the cleanliness obtainable from the coating process. The difference between the two process cycles reflects the degree of metallurgical continuity within the coating. Whilst peening deforms individual crystallites into closer contact, unless recrystallisation or metallurgical bonding can then take place the strains generated by the thermal shock will open up these regions of weak bonding and lead to early crack initiation, just as was observed.

It is worth noting that a sputter ion plated CoCrAlY coating offers a far greater thermal shock resistance than does aluminising. Whilst the life for the uncoated alloy to crack initiation is ~ 150-200 cycles, this is increased to ~ 300-500 cycles for the aluminised alloy. Again, a low pressure plasma sprayed Ni 35Co21Cr8Al-0.3Y (all wt.%'s) coating offers a life of ~ 600 cycles to crack initiation, illustrating the good performance and quality of the SIP coating process.

Moving closer to the conditions expected in a marine gas turbine, the corrosion resistance of some of these coatings has been determined in burner rig tests at temperatures between 700° and 900°C. However, the most convincing test vehicle is the engine itself. SIP coated turbine blades have been included, along with other coatings, in several recent marine gas turbine trials. In these tests which have extended out to several thousand hours, the gas turbine has been operated in a simulated marine environment under a variety of duty power cycles.

4. CONCLUSIONS

This paper started by considering the various features which a good coating system should possess. Whilst SIP coatings are not currently available on a commercial basis, the performance and potential of the

process has been amply demonstrated with the satisfactory performance of SIP coatings in laboratory oxidation and thermal fatigue tests. SIP therefore offers a simple alternative method for the deposition of MCrAlY overlay compositions and overcomes many of the shortcomings of the current commercial processes.

ACKNOWLEDGEMENTS

The authors are indebted to F. Cullen and B. Bellamy, AERE, for help with the X-ray diffraction experiments, and R.M.W. Hawes, AERE, for EPMA analysis. The help of Rolls-Royce Ltd. is kindly acknowledged.

REFERENCES

1. R.A. Dugdale, Proc. Int. Conf. on Ion Plating and Allied Techniques, (CEP Consultants, Edinburgh, 1977), p. 177.

2. D.M. Mattox and J.E. MacDonald, J. Appl. Phys. 34, 2493 1963.

3. R.D. Bland, G.J. Kominiak and D.M. Mattox, J. Vac. Sci. Technol. 11, 671 (1974).

4. D.H. Boone, S. Shen and R. McKoon, Thin Solid Films 64, 299 (1979).

5. D.K. Gupta and D.F. Duvall, Superalloys 1984, edited by M. Gell, C.S. Kortovich, R.H. Bricknell, W.B. Kent and J.F. Radavich, (Seven Springs, USA, 1984), p. 711.

6. S.J. Shaffer, D.H. Boone, R.T. Lambertson and D.E. Peacock, Thin Solid Films 107, 463 (1983).

7. B.C. Lippens and J.H. Boer, Acta Cryst. 17, 1312 (1964).

8. K. Wefers and G.M. Bell, Alcoa Research Laboratories, Technical Paper No. 19 (1972).

9. P.T. Moseley, K.R. Hyde, B.A. Bellamy and G. Tappin, Corrosion Science 24, 547 (1984).

10. W.K. Halnan and D. Lee, High Temperature Protective Coatings, edited by S.C. Singhal, (AIME, 1983), p. 3.

11. J.P. Coad and D.S. Rickerby, NATO Advanced Workshop on Coatings for Heat Engines (Acquafredda di Maratea, Italy, 1984).

Table 1

List of Coating Compositions (wt.%)

Coating	Co	Ni	Cr	Fe	Al	Ti	Si	Y
CoCrAlY	Bal	-	20	-	9	-	-	0.3
NiCrAlY	-	Bal	20	-	11	-	-	0.3
NiCrAlTi	-	Bal	35	-	8	3	-	-
CoNiCrAlY	Bal	24	22	-	9	-	-	0.3
FeCrAlY (Fecralloy*)	-	-	15	Bal	5	-	0.23	0.3

* Fecralloy is a registed trademark in the UK.

Table 2

Details of Thermal Shock Test

Maximum and minimum temperature	1020°C - 20°C
Radius of edge without coating	0.5 mm
Time in hot bed	4 mins
Time in cold bed	4 mins

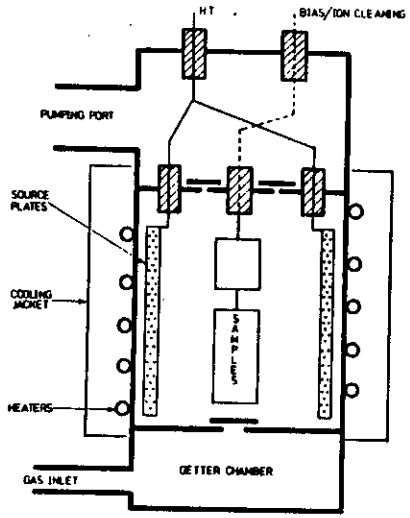

Figure 1 Schematic view of SIP system.

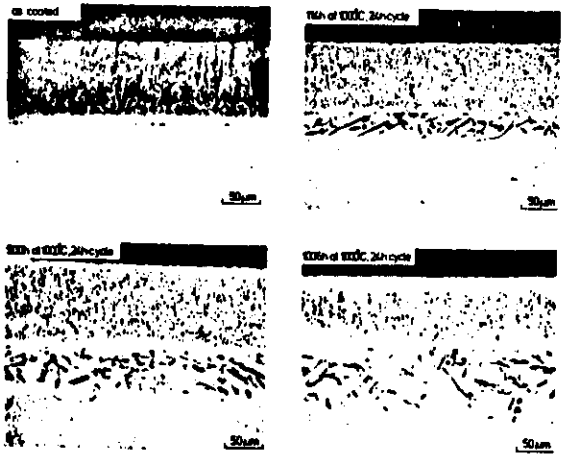

Figure 2 A CoCrAlY coating as-received, and after cyclic oxidation at 1000°C for periods of 114, 500 and 1006 h.

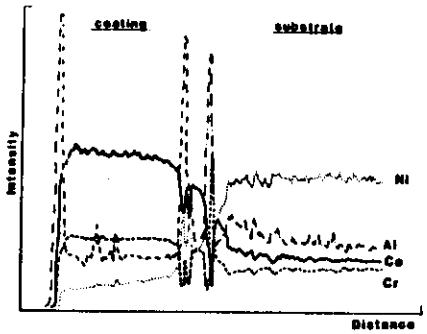

Figure 3 EPMA line profiles across a CoCrAlY coating on a nimonic alloy after 1006 h of cyclic oxidation at 1000°C.

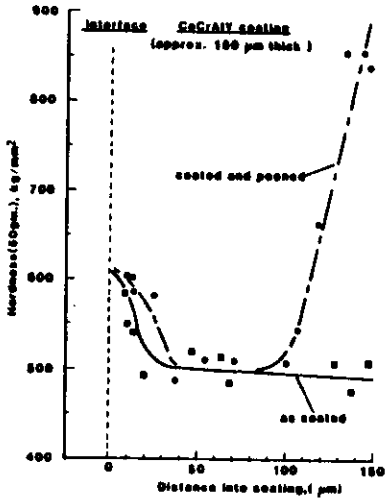

Figure 4 Microhardness profiles for a CoCrAlY coating, the distance into the coating being measured from the interface with the substrate.

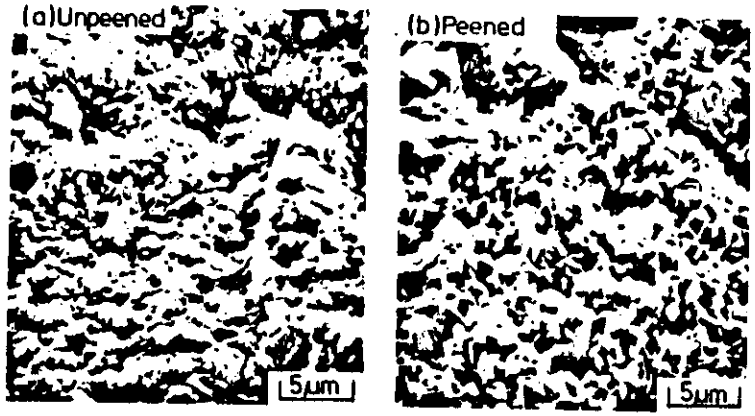

Figure 5 Oxide structures on a CoCrAlY coating after 6.5 h at 1000°C, (a) for an unpeened coating, and (b) for a coating peened before oxidation.

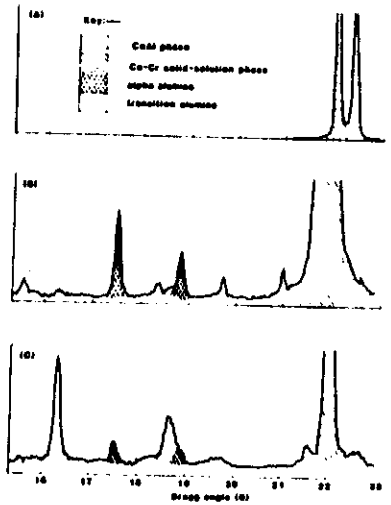

Figure 6 X-ray diffraction patterns of CoCrAlY coatings as-received and after isothermal oxidation at 1000°C for 6.5 h, (a) as-deposited, (b) unpeened prior to oxidation, and (c) for a coating peened before oxidation.

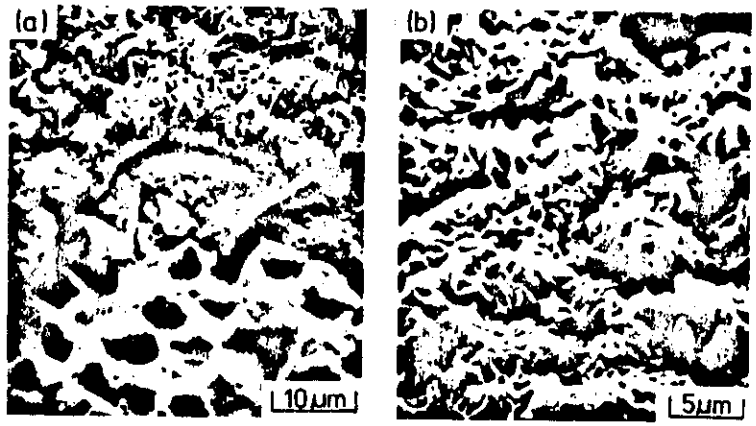

Figure 7 Oxide structures on a CoCrAlY coating after 100 h at 1000°C, (a) for a spalled region of the coating, and (b) an unspalled region.

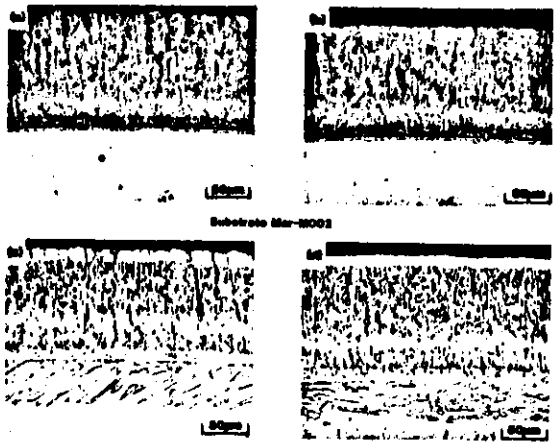

Figure 8 A CoCrAlY coating on a Mar-M002 corrosion pin before and after oxidation at 1100°C.

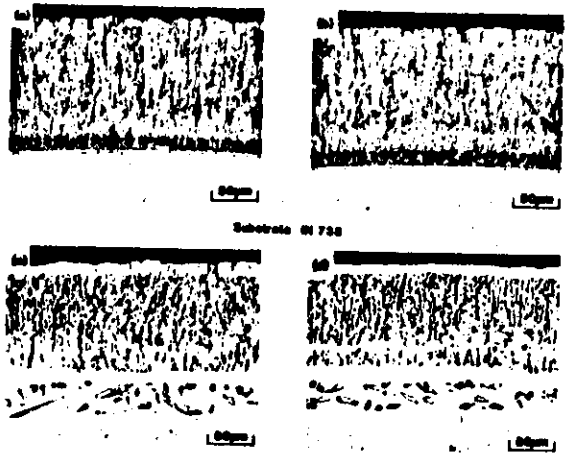

Figure 9 A CoCrAlY coating on a IN738 corrosion pin before and after oxidation at 1100°C.

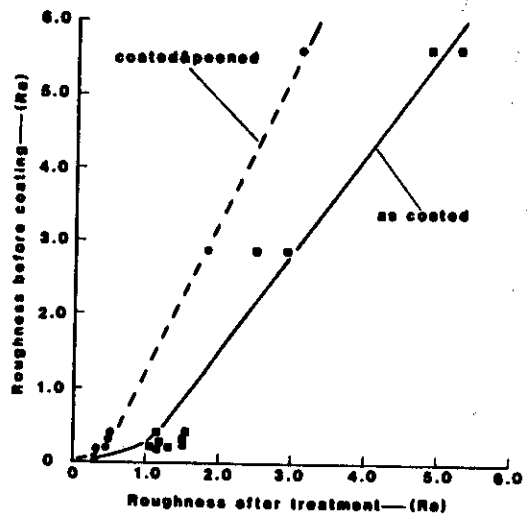

Figure 10 Influence of substrate surface roughness on the topography of CoCrAlY coatings: Results for as-coated IN792 corrosion pins shown thus: ■ ; for coated and peened thus: ●.

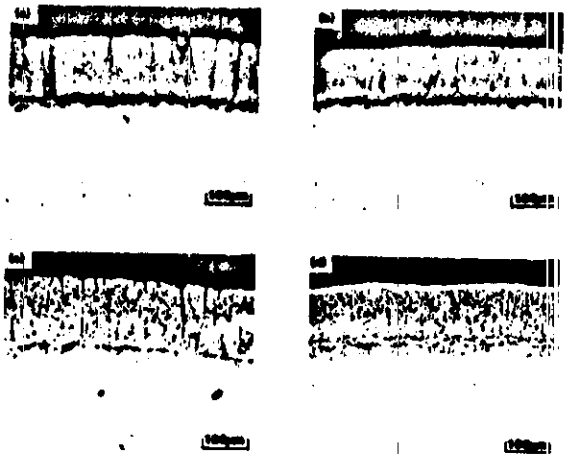

Figure 11 A CoCrAlY coating on a IN792 corrosion pin before and after oxidation at 1100°C; substrate surface roughness prior to coating ~ 3 µm.

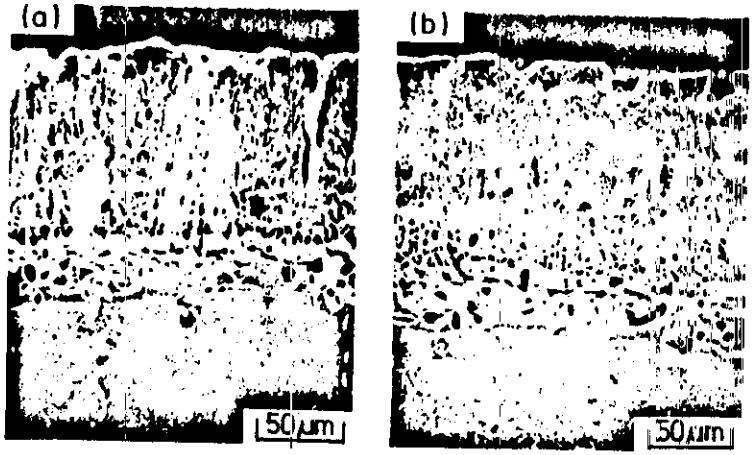

Figure 12 Secondary electron images of deep etched CoCrAlY coatings after oxidation at 1100°C, (a) for an unpeened coating, and (b) for a coating peened before oxidation.

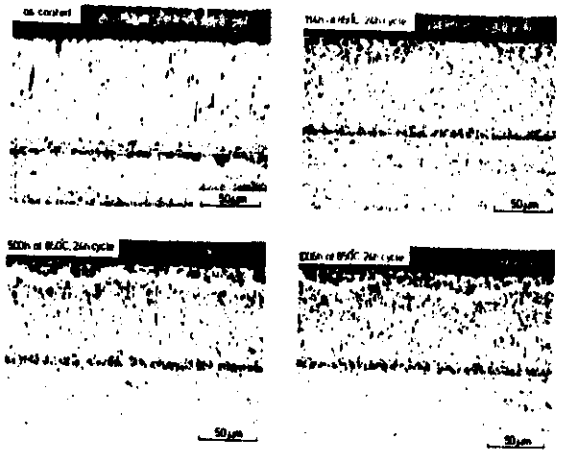

Figure 13 A NiCrAlTi coating as received, and after cyclic oxidation at 850°C for periods of 114, 500 and 1006 h.

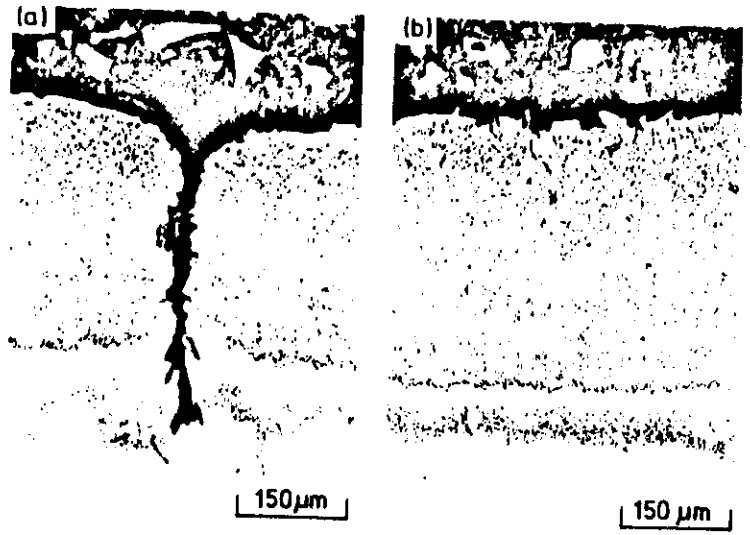

Figure 14 A CoCrAlY coating on a IN738LC thermal fatigue specimen after 1200 cycles.

AERE R 12360

United Kingdom Atomic Energy Authority

HARWELL

Bias, internal stress and substrate effects on the microstructure and properties of PVD-wear resistant coatings

D S Rickerby and P J Burnett

Materials Development Division
Harwell Laboratory, Oxfordshire OX11 0RA

October 1986

APPROVED FOR PUBLICATION

AERE R 12360

BIAS, INTERNAL STRESS AND SUBSTRATE EFFECTS ON THE MICROSTRUCTURE AND PROPERTIES OF PVD-WEAR RESISTANT COATINGS

D S Rickerby and P J Burnett*

ABSTRACT

The effect of the process parameter 'substrate bias' on the internal stress, microstructure and hardness of sputter ion plated titanium nitride coatings has been investigated. It is found that high bias levels results in coatings of fine grain size, high internal stress, low porosity and high hardness. The role of the thermal mismatch contribution to internal stress in densification of the coating is elucidated.

"Hardness anisotropy" has been observed when indenting plan and cross-sections of thick (~ 20 μm) TiN and WTiC coatings. An explanation for this behaviour has been proposed in terms of the microstructural anisotropy of the coatings coupled with the internal stress state acting within the test surface.

Scanning electron microscopy, transmission electron microscopy and X-ray diffraction studies of coating morphology, grain size, defect density and texture have been performed and the results obtained used to estimate the relative contributions of grain size and defect density to coating hardness using a simple Hall-Petch approach.

*On attachment from University of Oxford,
Department Metallurgy and Science of Materials,
Oxford, U.K.

Materials Development Division
Harwell Laboratory

October 1986

HL86/1437 (C14)

CONTENTS

TABLES

ILLUSTRATIONS

Figure 11 Hardness vs. indentation depth plots for (a) 1.7 μm unbiased TiN, (b) 1.65 μm of TiN (-10 V bias), (c) 1.2 μm of TiN (-35 V bias) and (d) 1 μm of TiN (-50 V bias) onto stainless steel substrates. The data points (• O) are the experimentally determined composite hardness (open symbols representing measurements made from oblique illumination light micrographs), the data points (■) are the measured substrate hardness values. Curves 1 are the substrate hardness behaviour assumed in subsequent calculations. Curves 2 are the "true" coating hardness behaviour assumed for calculation and curves 3 are the predicted hardness variation derived from curves 1 an 2 using the Burnett and Rickerby hardness model[21,22]. Good fits are achieved in all cases.

Figure 12 Variation of the interface parameter χ vs. $(E_f H'_s / H'_f E_s)^{\frac{1}{2}}$ (the ratio of plastic zone sizes at a 10 μm indent size), used to obtain the fits in Figure 11. Note that all points are consistent with the trends derived from previous work.

Figure 13 The hardness (50 gf, Vickers) of FeCrAlY (■) and CoCrAlY (•) coatings as a function of distance from the coating/substrate interface obtained from indentation of metallographic cross-sections. Note that the Zone 1 structure of the FeCrAlY coating results in a softening towards the surface whilst the denser Zone 2 structure of the CoCrAlY coating results in an almost constant hardness.

Figure 14 (a) An etched metallographic cross-section of a FeCrAlY coating (similar to that used to obtain the hardness data for Figure 13) showing a Zone 1 type microstructure. Schematic variation of (b) hardness, (c) internal stress and (d) density with distance from the coating/substrate interface for Zone 1 microstructures (shaded bands) and Zone 2 microstructures (open bands). Note that for Zone 1 microstructures all three quantities decrease with distance whilst they are expected to remain approximately constant for Zone 2 microstructures.

Figure 15 The measured Knoop hardness values for a WTiC coating on A30 cemented carbide and austenitic stainless steel using three indenter orientations. Note the greater hardness of the orientation C in both cases.

Figure 16 (a) Schematic representation of the suggested deformation morphology of a PVD coating beneath a hardness indenter (orientation C in Figure 15). When indenting the columnar structural units "end-on" the columns expand and interact with their neighbours (see insert) once these interactions have occurred the neighbouring columns effectively constrain any further expansion. Thus, coatings with low levels of intercolumnar porosity will appear harder than those with high porosity.
(b) A schematic representation of the stress-state acting in the coating shown in (a). Stress orientation as in insert in (a).

Figure 17 (a) Schematic representation of the suggested deformation morphology of a PVD coating beneath a hardness indenter when indenting in cross-section (orientations A and B in Figure 15). Preparation of the cross-section releases the σ_{yy} compressive internal stress component close to the test surface (see (b)) which can result in the "opening up" of the columnar units towards the new surface (as indicated by the large shaded arrow). Indentation in this orientation can then result in densification of the columns together with sliding of the weak grain boundaries and buckling of the columns. This results in a low hardness compared to the "end-on" indentation of Figure 16.

(b) A schematic representation of the stress-state acting in the coating shown in (a). Stress orientation as in insert. Note that for a given depth into the coating the internal stress component σ_{yy} decreases towards the test surface whilst σ_{xx} remains relatively unaffected by the presence of the new free surface.

Figure 18 Bright-field electron micrograph of a TiN film stripped from its M2-tool steel substrate.

Figure 19 Bright-field electron micrograph of a TiN film stripped from its martensitic-420 stainless steel substrate.

Figure 20 Bright-field electron micrograph of a TiN film stripped from its austenitic stainless steel substrate.

Figure 21 Bright-field/dark-field pair of a region of TiN coating stripped from martensitic-420 stainless steel substrate showing a high density of defects thought to be dislocation loops.

30 d

1. INTRODUCTION

The increasing importance and use of surface coatings in tribological applications brings with it a need for a fundamental understanding of their properties if the optimum coating for a particular purpose is to be selected. Furthermore, in order to produce coatings tailored for specific tasks a knowledge of the inter-relationship between process or system parameters (for example, substrate bias) and coating properties (e.g. hardness) needs to be determined. Of the wear-resistant coatings, titanium nitride is finding an increasing range of applications in addition to its use on drill bits[1] and tool materials[2,3]. This material, produced either by chemical vapour deposition (CVD) or physical vapour deposition (PVD) techniques, is usually deposited as films of 1-10 μm in thickness and has been shown to be beneficial to wear resistance[1-3].

In this paper we shall consider only PVD coatings produced by the process known as sputter ion plating (SIP)[4,5]. This class of coating is becoming of increasing interest as it is possible to deposit films at temperatures substantially lower than those used for CVD ($\lesssim$ 550°C against $\gtrsim$ 800°C) and thus coating of heat-sensitive substrates becomes feasible[6]. Many studies have been published concerning the properties and structure of PVD-TiN (and other wear-resistant coatings)[e.g.7-11]. In these previous studies, the tribologically important parameter of hardness has been correlated with stoichiometry[7-9], the presence of porosity/ voids[7,10,11], both at the grain boundaries and within the grains themselves, and the degree of ion-bombardment that the workpiece undergoes during coating, whilst other properties such as electrical resistivity have been correlated to grain size, stoichiometry (purity[12]) and defect density[7,8]. In addition to these parameters, quantities such as internal stress (a combination of thermal mismatch and intrinsic growth stresses) may also be important in determining the wear-resistance of PVD coatings. The rôle of internal stress in determining coating adhesion has been extensively discussed[e.g.13-15] but, in contrast, the rôle of internal stress in determining the nature of the final coating microstructure has been relatively neglected. However, Aubert et al.[16] have correlated compressive internal stress with the density of magnetron sputtered molybdenum and Rickerby[13] has

suggested similarly that compressive internal stresses may be of paramount importance in determining the porosity of titanium nitride and other hard PVD coatings. Thus, internal stress may constitute another, previously unconsidered, degree of freedom in the construction of PVD coating structure models such as those described by Movchan and Demchishin[17] with modifications due to Thornton[18].

In PVD processes such as ion-plating the application of a substrate bias makes it possible to control the degree of ion-bombardment the coating experiences during growth, which in turn affects the density, grain size and growth morphology of PVD coatings[7,12,19]. Importantly, surface mobility increases with ion-bombardment flux and this aids the nucleation stage of film growth resulting in a coating of higher density, higher defect density and smaller grain size and, in extremis, a loss of columnar microstructure[e.g.20]. Recent work[13] has also shown that internal stress increases with bias voltage due to a concomitant increase in density. Consequently, substrate bias may also be expected to affect properties such as hardness by controlling porosity, defect density and grain size.

Clearly, all the properties, process parameters and microstructural characteristics described briefly above, are inextricably linked. Furthermore, these are not the only quantities that may determine the ultimate behaviour of a PVD coating. Factors such as growth rate, deposition temperature, etc., all play a major rôle. However, we shall not discuss these here, rather, it is the aim of this paper to review and develop ideas on mechanical properties and structure relationships and to correlate these explicitly with process and system parameters.

The variation of internal stress and microstructure with substrate bias will be presented together with both scanning electron microscopy (SEM) and transmission electron microscopy (TEM) studies of the morphologies of the titanium nitride coatings deposited onto a variety of substrate materials. The variations of hardness with bias will be determined using the volume law-of-mixtures hardness model, as proposed by Burnett and Rickerby[21,22], for the determination of "true" thin film hardness values. The variation of hardness ("hardness anisotropy") of coatings when tested in through-thickness (plan) and in cross-section

will be described and deformation mechanisms proposed to account for these effects. An attempt will be made to describe the way in which the process parameter, 'substrate bias' and (principally) system parameter, 'internal stress' determine the microstructure of the coating and the resultant mechanical properties. Finally, the relative importance of grain size and defect density on the hardness of PVD-TiN will be discussed.

2. EXPERIMENTAL

2.1 Sputter Ion Plating

SIP[4,5] is a coating technique which enables a coating to be built up from a flux of atoms and ions which have been sputtered from solid source plates. The equipment consists of a chamber which is lined with coating source plates and which act as the cathodes for the glow discharge, a mechanical pump for evacuating the unit, a getter and a suitable power supply. The components to be coated are suspended within the volume enclosed by the source plates and are held at a small negative voltage during deposition to control the structure of the coating[7,20]. The coating compartment and its contents are pre-heated to about 300°C to outgas all the exposed surfaces and to enable the establishment of a very pure atmosphere which is important for good coating adhesion. To enhance adhesion the samples may be cleaned by ion bombardment, if desired, to remove the thin surface oxide layers and a thin metallic interlayer deposited to further improve adhesion. An argon glow discharge is then set up within the chamber by applying a negative voltage of approximately 1000 V to the cathodes. Atoms and ions are sputtered off the cathodes (the coating source plates) and form a flux of material which settles on the components (and exposed parts of the chamber) to produce the coating. In the reactive sputtering mode, titanium source plates are sputtered in the presence of an Ar/N_2 gas mixture to form titanium nitride at the surface of the component to be coated. The relatively small bias voltage on the components (0-100 V) results in "ion polishing" of the coating surface to promote a dense structure and also serves to refine the composition of the nitride[12].

SIP may be used to produce coatings of complex alloys by the provision of source plates of suitable composition (see Ref. 23 for further details).

In the present study SIP was used to deposit titanium nitride onto a number of austenitic and ferritic steel coupons to thicknesses in the range 1-10 μm using negative bias voltages of 0 to 50 V. In addition to the titanium nitride coatings, tungsten-titanium carbide films were also produced (using mixed W/Ti source plates and an Ar/CH_4 gas mixture), the thickness of these coatings being ~ 20 μm. Coatings of pure metals (molybdenum) and alloys (MCrAlY composition where M is Ni, Co or Fe) were also deposited under Zone 1 (Fecralloy* and molybdenum) and Zone 2 (CoCrAlY) conditions to investigate the effects of coating temperature on the microstructure of PVD deposits.

2.2 Microhardness Testing

Microhardness testing was performed with a Shimadzu microhardness tester using loads between 15 gf and 1 kgf and a dwell time of 15 seconds. In addition to the usual through-thickness studies on coated coupons, microhardness tests were also carried out on metallographically prepared cross-sections in order to study any "hardness anisotropy" effects in these coatings. Measurements of indentation size were made using the optical system of the microhardness tester and from photomicrographs taken at x2.5 k magnification (n.a. = 0.95) using oblique illumination. This latter method was found to highlight the edges of indentations and enabled measurements to accuracies in excess of those usually attainable using normal incidence illumination. For all hardness measurements, approximately ten diagonals were measured at each load and the hardness numbers calculated from the means and standard deviations of these values.

Analysis of the through-thickness hardness data was performed using the model proposed by Burnett and Rickerby[20,21] for hard wear-resistant coatings, which allows contributions to the measured hardness from the coating and substrate to be identified. The "true" coating hardness is derived using the expression:

$$H_c = \frac{V_f}{V} H_f + \frac{V_s \chi^3}{V} H_s \qquad \text{for } H_f > H_s \qquad (1)$$

where H_c, H_f and H_s are the hardness values of the composite (i.e. the measured hardness), the film and the coating respectively; V_f and V_s are the deforming volumes beneath the indentor of the film and substrate respectively (so $V = V_s + V_f$) and χ, termed the "interface parameter", is a measure of the constraint imposed by the harder coating on the deformation of the softer substrate at the interface and is given approximately by:

$$\chi = 0.08 + 1.099 \left(E_f H_s'/E_s H_f'\right)^{\frac{1}{2}} \qquad (2)$$

where E_f and E_s are the Youngs moduli of the film and substrate respectively and H_s', H_f' are the hardness of the substrate and coating at a given indentation size (usually 10 μm).

In this model the hardness values used incorporate indentation size effect (ISE) terms since it is expected that the PVD coatings will exhibit a marked dependence of hardness on load (or diagonal) in common with other ceramic materials[24]. The Meyer Law ISE formulation[24,25] is used whereby:

$$H_d = a d^{m-2} \qquad (3)$$

where H_d is the hardness at diagonal d, 'a' is a constant and m the ISE index. To completely define the hardness at all indentation sizes we need only specify the hardness at a known diagonal size (usually 10 μm, i.e. $H_{10\ \mu m}$) and the constant 'a'.

---

* Fecralloy is a registered trademark of the United Kindom Atomic Energy Authority.

2.3 Electron Microscopy

Scanning electron microscopy studies (using a Hitachi S-520 SEM operated at 20-30 keV) were performed on both plan-sections (i.e. as-coated surface) and fracture cross-sections of the coatings.

Transmission electron microscopy was carried out using a Philips EM400T operated at 100 and 120 kV. The samples were prepared by first dissolving away the substrate in a 10% bromine in methanol mixture and then mounting the free-standing film on a 3 mm copper keyhole grid prior to ion-beam thinning to electron transparency with a 5 kV Ar^+ beam.

2.4 X-ray Stress Measurement

The internal stress present in the TiN coatings was measured by the $\sin^2 \Psi$ method[26] using Cu Kα radiation on a Philips diffractometer. High angle diffraction peaks were used where possible to ensure a high precision. Full experimental details can be found elsewhere[13,27].

3. RESULTS AND DISCUSSION

3.1 Bias Effects

In this section we shall explore the ways in which substrate bias can influence (i) internal stress, (ii) microstructure and (iii) microhardness. Finally, we shall summarise the results of these sections.

3.1.1 The Effect of Bias on Internal Stress

For titanium nitride deposited onto an austenitic stainless steel, the level of compressive internal stress increases with bias voltage as shown by Figure 1 (see also Ref. 13) and depends upon (i) the density and (ii) the yield strength of the film. [This latter quantity will depend to some extent upon the grain size; since it is known that high biases decrease grain size, which from a simple Hall-Petch approach would bring about an increase in the yield stress of the coating (see Section 3.4).] By way of comparison Table 1 lists the measured internal

stresses for SIP (-35 V substrate bias) and ion plated titanium nitride coatings (data from Ref. 28). Clearly, the stress in a SIP coating is somewhat greater than the stress component which could be generated due to differences in the thermal expansion coefficients of substrate and coating alone, and this has been attributed to the presence of an intrinsic or growth stress. However, it is worth noting that for ion-plated titanium nitride the high bias levels used in ion plating ($\sim$ 500-2000 V) would (on the basis of Figure 1) be expected to produce much higher levels of internal stress due to an increased contribution of the intrinsic or growth stress contribution to total internal stress. Furthermore, it is interesting to note that, both in the present study and for ion-plated titanium nitride, the average stress level in the coating decreases with increasing coating thickness. This, we believe, is related to the changing structure/density of the coating as it grows, a point which will now be dealt with in some detail.

3.1.2 The Effect of Bias on Microstructure

Application of a substrate bias during the deposition of a coating has a profound effect upon the growth and resultant microstructure of PVD films. Figure 2 shows fracture sections through unbiased and biased SIP-TiN films. The unbiased film (Figure 2a) clearly shows an open columnar structure (a Zone 1 type microstructure) whilst the biased film appears much more dense, the individual columns being much less well defined (Zone T type structure). Figure 3 shows higher magnification views of the surface topography of these specimens. The unbiased specimen (Figure 3a) shows the columns to be faceted, generally terminating in tetrahedral structure (this is consistent with a {111} texture, see Section 3.3.1), again large gaps are evident between the columns. In contrast, the biased specimen (Figure 3b) shows much smaller, rounded ends to the columnar structures, with no obvious gaps between the structural units which make up the coating. Both Figures 2 and 3 support the previous reports that bias both densifies the coating and reduces the grain size[e.g.7-11]. This apparent increase in the density of the coating with substrate bias has been reported previously by one of us (Rickerby[13]) and can be correlated to the levels of internal stress present in the coatings. Figure 4 compares tungsten-titanium carbide coatings ($\sim$ 20 μm thick) both

adherent to a stainless steel substrate (Figure 4a) and free-standing (Figure 4b). On removal of the constraining substrate the internal stress present in the plane of the coating is relaxed and so the columnar structure becomes apparent in the free-standing film, the intercolumnar voids extending to the coating/substrate interface (Fig. 4b), this microstructure now being consistent with the structure models of Thornton[18]. In contrast, in the adherent (strained) coating the columnar units are only apparent close to the surface where it is expected that the coating becomes more open with a concomitant reduction in the level of internal stress (see Sections 3.1.1 and 3.2). The affects of stress in densification of coatings can be very clearly demonstrated using SIP molybdenum coating onto (i) molybdenum and (ii) stainless steel substrate. Clearly in (i) there will be no thermal mismatch and so the internal stress will be low for Zone 1 type deposition conditions. However in (ii) there is substantial thermal mismatch ($\Delta\alpha = 10 \times 10^{-6}\ ^{\circ}C^{-1}$) and a large compressive stress will develop on cooling from the deposition temperature (of approximately 500°C). Figures 5 and 6 show fracture cross-sections for these two cases and, as expected, the Mo onto Mo coating (internal stress measured as 100-200 MPa) appears open and fibrous (Figure 5) whilst the Mo onto stainless steel coating (internal stress of approximately 1000 MPa) appears denser and the columnar units, whilst still visible (see Figure 6), appear to have few gaps between them. Since these specimens were coated in the same run all other process variables are assumed identical so the differences in structure must be a manifestation of the stress state and confirm the importance of internal stress in densification of hard wear-resistant coatings.

Thus, the process variable of substrate bias will refine grain size, may alter columnar morphology and will act to produce denser coatings by virtue of increased surface mobility and enhanced nucleation kinetics. Denser coatings mean that high internal stresses may be supported, whilst for unbiased coatings, where each column is an island surrounded by space, little or no stress can be supported since the columns do not interact with their neighbours and have to be brought together before they can transmit stresses. In addition to bias effects, the systems variable of coating/substrate combination can enhance densification if the thermal expansion of the substrate is

greater than that of the coating. In this case, on cooling the columnar units will be brought together and a compressive internal stress set up. This may then act to further densify the coating resulting in a very dense microstructure such as that in Figure 4a. In summary, if bias voltage is increased the intrinsic of growth stress component also increases, and by virtue of the better microstructure substantial thermal mis-match stresses can be generated. However, the opposite state-of-affairs may exist in which the thermal stress may be tensile and this can cancel the compressive growth stress and so result in a very low residual internal stress on cooling from deposition temperature as shown in Table 1 from titanium nitride coatings deposited onto a cemented carbide.

3.1.3 The Effect of Bias on Hardness

Coating microstructure depends critically upon bias voltage and this in turn affects the way in which the coating can respond in any given situation, e.g. during indentation testing. Figure 7 shows indentations made in unbiased (Figure 7a) and -35 V biased (Figure 7b) TiN coated stainless steel. For the unbiased sample, little cracking is in evidence, although smearing and densification is readily apparent, particularly along the edges of the indentation and at the apex of the incent. [Figure 3a shows this smearing and densification at higher magnification.] Conversely, for the biased specimen (Figure 7b) cracking is evident around and within the indentation, the cracking appearing most marked in those areas in which smearing was apparent in (a), these regions being those that suffer the greatest stresses during indentation. The nature of the substrate may also affect the mode of deformation. Figure 8 shows 100 gf indentations made in titanium nitride deposited on austenitic steel and M2-tool steel. In the former (Figure 8a), cracking within the indent and to some distance outside of the impression is apparent whilst in the latter much less cracking is evident and it is contained entirely within the impression.

The reason behind this difference may be easily understood by reference to Figure 9. The hard M2-tool steel behaves as an elastic/plastic substrate and displaced material is removed by radially directed plastic flow until the displaced volume is spread over a sufficiently

large yield front that it may be accommodated elastically (this being the spherical cavity model for indentation[29]). The coating will also deform in a radial manner, these processes being described in greater detail elsewhere[20,21]. In contrast, the soft stainless steel behaves as a rigid/ plastic substrate for which the Tabor relation[25] holds thus:

$$H \propto 3Y \qquad (4)$$

Rather than undergo radial displacements during indentation, these materials "pile-up" the displaced material around the indentation forming a lip (Figure 10) which is shown schematically in Figure 9. Clearly, the shear stresses that arise because of this vertical motion may be sufficiently large to shear the coating along its grain boundaries (these being weak) giving rise to cracking away from the indentation as in Figure 8a. For unbiased coatings such as Figure 7a the individual "islands" of material merely move up and down with the substrate - although the individual 'islands' of material are adherent to the substrate, they do not form a continuous coating and therefore cannot crack.

Microhardness tests were performed on titanium nitride coatings deposited onto an austenitic stainless steel at four bias levels and the data analysed as described in Section 2.2. The best fit $H_{10\ \mu m}$ values obtained using this procedure are shown in Table 2 and plotted against bias in Figure 1. A selection of experimental data and the predicted fits using the parameters in Table 2 are shown in Figure 11. Good fits are achieved in all cases. The values of interface parameter, χ, used to obtain these fits are plotted in Figure 12 and it can be seen that these are consistent with values obtained for other coating/substrate systems previously studied[20,21]. From Table 2 it can be seen that in order to fit the hardness model to the experimental data it was necessary to vary the effective elastic modulus of the coating considerably. This is not surprising since, for the less dense, low bias coating the effective elastic modulus will reflect the relative levels of porosity in TiN coatings. Once fully dense coatings of TiN have been established the elastic modulus of bulk TiN is required.

As mentioned in Section 3.1.1, the average internal stress present in PVD-TiN coatings generally decreases with increasing thickness, this being consistent with the structure becoming less dense as it grows outwards. Thus, thicker coatings of otherwise similar material, might be expected to appear softer than thinner coatings since the indentation will be sampling greater porosity[20,21]. Due to the thinness of the PVD-TiN coating, it is impossible to study this directly using metallographic cross-section, however, it is possible to obtain microhardness profiles on cross-sections of thicker ($\sim$ 100 μm) MCrAlY coatings, and Figure 13 shows such data obtained for a Zone 1 type structure Fecralloy coating and a Zone 2 type structure CoCrAlY coating, both deposited by SIP. The Zone 1 structure, as defined by Thornton[18], consists of columnar crystallites with open boundaries (see Figure 14a). These open boundaries develop as certain favourably oriented crystallites grow out into the vapour phase at the expense of other crystal nuclei that may have formed on the substrate. Thus, the material at the interface is finer grained and more dense than the large, widely spaced columns that eventually constitute the structure some distance from the interface (see Figure 14a). This growth morphology was recently shown by Helmersson et al.[30] for reactively sputtered (TiN), so the MCrAlY type materials appear to parallel the behaviour of PVD wear-resistant coatings. From Figure 13 it can be seen that the hardness of the coating decreases with increasing distance from the interface. In contrast the Zone 2 CoCrAlY coating (defined as consisting of columnar crystallites separated by dense inter-crystalline boundaries) shows little change in hardness. Figure 14(b-d) indicates schematically how hardness, internal stress and density are expected to vary with distance from the interface. For Zone 1 (the shaded bands in Figure 14(b-d) and to a lesser extent Zone T type PVD-structures, all three of these quantities decrease with distance from the interface. The expected variations of these properties for Zone 2 structures are also shown for comparison (open bands). Here, little change in hardness, internal stress and density are expected. Since bias can determine the density and growth morphology of a titanium nitride coating (Section 3.1.2) (the structures varying from open Zone 1 type (e.g. Figure 3a) to dense Zone T/Zone 2 type) it is expected that these PVD-TiN coatings will exhibit variations of

hardness, internal stress and density akin to those observed for the MCrAlY coatings. Accordingly, Figure 14(b-d) may be considered to represent the low bias case (shaded bands) and high bias case (open bands).

This section has attempted to indicate the interdependence of bias, microstructure, mechanical properties and internal stress. In addition, the deformation modes associated with indentation and the influence of the substrate have been discussed. Bias has been shown to refine the grain size, promote densification and increase internal stress levels (both by virtue of increasing growth stress contribution and providing a dense coating for thermal mismatch stress to act within). The thermal mismatch between coating and substrate has also been shown to be able to substantially affect the coating structure, those combinations of coating and substrate that result in high thermal compressive stresses acting to densify the coating. Finally, the consequence of the microstructural effects of bias upon hardness have been discussed and it has been shown that hard coatings result from high bias levels.

3.2 Hardness Anisotropy

The apparent discrepancy between the hardness of PVD coatings measured in cross-section and through-thickness has been reported by us and others previously[20,21,31]. This will now be discussed further.

Figure 15 shows typical Knoop hardness data obtained by indenting thick (~ 20 μm) PVD wear-resistant coatings both through thickness (orientation C) and in cross-section (orientations A and B) on metallographically prepared sections. It can be seen that irrespective of substrate the hardness in cross-section was significantly less than that in through-thickness. In a previous paper[20,21] we suggested three possible reasons for this behaviour:

(i) Microstructural anisotropy.

(ii) Crystallographic anisotropy.

(iii) Differences in internal stress.

We suggest that it is a combination of (i) and (iii) that is responsible for this effect as follows.

With reference to Figure 16, during through-thickness indentation the columns are compressed along their axis. Since the action of the compressive internal stresses (shown schematically in Figure 16b) is to push the columns together, these columns will be constrained by their neighbours, except maybe near the surface where the coating becomes more open (Section 3.1.3). Thus, any deformation that occurs within the columns will be additionally constrained by further interaction with their neighbours (see inset Figure 16a). Consequently, deformation is difficult and the coating appears hard (in contrast, open unbiased coatings lack this constraint and the columns are easily deformed or pushed to one-side). However, in the cross-section the stress state is markedly different (Figure 17b), since the internal stress acting normal to the indented surface (σ_{yy}) must fall to zero at that surface, consequently the stress induced packing of the columns is lost resulting in the columns moving apart towards the test surface. Consequently, σ_{xx} parallel to the surface is retained and relatively unaffected, whilst σ_{zz} (the tensile stress normal to the interface) is somewhat reduced. Now, upon indentation (Figure 17a), the loosely packed columns are indented across their axis and may buckle or crack. In addition, their loose packing and weak grain boundaries may slide over one another allowing both plasticity and densification. Thus, the coating appears softer than the through-thickness hardness. It is worth noting that coatings that exhibit a fine, e.g. equiaxed grain structure (such as those produced by CVD processes) do not show a hardness anisotropy effect[31].

Crystallographic texture may also contribute to the hardness anisotropy effect since it is known that PVD coatings often grow with a preferred orientation[7,13] (see 3.3.1).

3.3 The Influence of Substrate on Coating Microstructure

3.3.1 Texture

Films grown by PVD techniques have been reported to exhibit a preferred growth orientation. For TiN films a {111} orientation is commonly reported although both {200} and {220} orientations have also been found by some workers[7,30]. The development of textures in PVD coatings occurs in three stages:

(i) Nucleation - crystallites are nucleated on the substrate from the vapour phase. The distribution, orientation and size of which will depend on the nature of the substrate.

(ii) Competitive growth - certain favourably oriented nuclei will grow faster into the vapour phase than the remainder of the crystallites. However, these may not constitute the majority of the nuclei population.

(iii) Steady growth - once a preferred orientation has achieved dominance, steady-state growth will occur.

In the present study, X-ray techniques and electron diffraction in the TEM were used to study texture developed in titanium nitride films deposited onto M2-tool steel, martensitic-420 stainless steel and austenitic stainless steel. Selected area diffraction patterns (SADPs) obtained from these three films (once the substrate had been dissolved away) are shown as the insets in Figures 18-20 respectively. In the SADPs from the TiN films on the M2 and 420 steels (Figures 18 and 19) the first well-defined diffraction rings are the {200} reflections, only a few {111} reflections being found within these rings. In contrast, in the SADP for the coating stripped from the austenitic stainless steel the {111} ring is readily apparent. These observations indicate that for TiN on M2 and 420 steel substrates that a {200} texture is present whilst for the austenitic stainless steel substrate the presence of the {111} reflections (indicating $\{2\bar{2}0\}$ planes parallel to the surface) means that all rings appear of approximately equal populations suggesting a random texture. Note that these observations are only

representative of the microstructure at the depth within the film from which they were taken, in this case from the central portion of films originally ~ 5 μm thick.

Table 3 summarises the texture coefficients, T^*, obtained for TiN (at three thicknesses) on various substrates, these being derived from relative X-ray peak intensity measurements which, unlike the TEM studies above, are an <u>average</u> of the texture throughout the thickness of the film. These data qualitatively agree with the SADP observations in that the M2 steel appears to have a stronger {200} texture, at a given thickness, than the austenitic stainless steel, the converse being true for the {111} texture. However, the data does not bear close examination, scatter between samples being large (see Ref. 27 for full analysis of this data), but does serve to show that the {111} texture develops at the expense of the {200} and {220} textures as the coating thickens. This is what would be expected for an fcc material such as TiN where the {111} phase is of lowest surface energy[30].

The effect of preferred orientation upon coating microstructure can be clearly seen in Figure 3a which shows an unbiased TiN film with a strong {111} texture (as confirmed by X-ray methods) exhibiting faceted growth. The pyramidal end forms on the columns are likely to be the low energy {111} planes. Thus, it would appear for all specimens studied that a {111} texture will eventually be developed if the coating is allowed to grow to sufficient thickness. Thinner coatings show {200} textures indicating that this is the predominant orientation at nucleation.

3.3.2 Grain Size

Clearly, from Figures 18-20, the grain sizes of TiN from M2 steel and austenitic stainless steel are similar (~ 70-100 nm) but that of the TiN grown on martensitic 420 stainless steel appears much larger (200-300 nm). It is not clear in absolute terms what governs the grain size. Since all three TiN films in Figures 18-20 were deposited under similar conditions the effects of bias, vapour flux, etc., can be eliminated. Thus, the substrate appears to have a strong influence over grain size and this may be determined by the availability of suitable

heterogeneous nucleation sites on the substrate such as grain boundaries and inclusions as well as the crystal structure of the substrate. With regard to the latter point, it is interesting to note that the finer grain sizes were nucleated on austenitic and ferritic steels and the coarse grain strucutre on a ferritic steel, this implies the crystal structure plays a minor rôle in nucleation in this case. In the present studies, titanium interlayers have been used to improve the adhesion of titanium nitride to the substrate and the effect of these Ti interlayers upon nucleation is unclear[32]. Upon deposition, Ti interlayers have been observed to form as large grains[32], yet the TiN nucleated upon this layer has a very fine grain size. Thus, it may be that the thin Ti interlayers used here (< 1000 Å) replicate substrate features which can then act as nucleation sites.

3.3.3 Defect Structure

It is often stated that PVD TiN coatings are hard because of the presence of a high density of defects such as dislocations, vacancy loops, argon entrapment, etc. (see Sections 3.2 and 3.4). In contrast, Sundgren[7] has reported that in certain PVD TiN coatings the presence of grain boundary voids is responsible for the poor mechanical properties of these coatings. No such voids may be seen in Figures 18-20, nor were any observed during the course of this study. However, Figures 18-20 all show some defect contrast within the grains. In particular, the TiN coating stripped from martensitic-420 stainless steel substrate (Figure 19) shows high densities of defects when compared to the coating stripped from the M2-tool steel (Figure 18). Figure 21 is a bright field/dark field pair of an individual titanium nitride grain and shows strong defect contrast similar to that obtained from dislocation loops.

These differences in defect density are reflected in the X-ray peak-broadening or "microstrain" measurements. Upon removal of the coating from the substrate the microstrains present in the TiN on M2-tool steel relax, those present in the TiN on coatings stripped from martensitic-420 and austenitic stainless steels remain substantially unchanged (see Table 4). Rickerby[13] suggested that the microstrains present in the TiN/M2 system were due principally to interaction at the

grain boundaries under the action of the internal stress whilst those present on the TiN/stainless steel systems also included a major contribution from the presence of defects such as the dislocation loops found within the individual grains of titanium nitride and shown in Figure 21. Table 4 summarises the microstrain data determined for both adherent and free-standing films together with the internal stress levels measured for coatings of similar thickness. The difference in defect density between the M2 and martensitic-420 steels may be explained in terms of the grain size dependency of yield stress. Since the TiN on martensitic-420 stainless steel coating possesses a larger grain size than TiN on M2 or austenitic stainless steel, according to the Hall-Petch equation (see section 3.4), its yield stress will be lower than the other coatings. Consequently, under the action of an imposed compressive internal stress this film may yield resulting in the formation of high densities of defects such as the loops observed. Conversely, under a similar internal stress the TiN on M2 film would fail to yield since its smaller grain size results in a higher yield stress. It should be noted that the thermal contribution to stress is similar for both substrates. The defects in fine grained TiN on austenitic stainless steel probably arise from plastic yield, as for the martensitic-420 steel. However, the presence of a much greater internal stress (due principally to greater thermal mismatch) results in the yield stress of the stronger fine grained coating now being exceeded. Note, that the very presence of the defects in the coarse grained material will act to raise its effective yield stress by "work-hardening".

In summary, TEM has shown that the columnar structural units of SIP-TiN consists of groups of fine (< 300 nm) approximately equiaxed (in the plane of the section) grains that generally show some defect contrast within them. The observation of pyramidal, faceted end forms to the columns in the unbiased TiN, indicates that on occasion the columnar units may be single crystals. The precise size, defect density and texture present has been shown to be a function of the substrate, although the precise mechanism by which the substrate exerts control over the microstructure is unclear.

3.4 Factors Affecting the Hardness of PVD-TiN

Given the observations described above, it is of interest to consider why these PVD-coatings are so hard. A review of the literature often finds assertions that the high hardness of these coatings is due to increases in defect density brought about by an ion bombardment and/or the establishment of a very fine grain size. Using a simple Hall-Petch approach the yield stress, σ_y, may be expressed as:

$$\sigma_y = \sigma_o + kd^{-\frac{1}{2}} \qquad (5)$$

where $$k = M_2 \left[\frac{M_1 G \tau_c b}{\pi (1 - \nu)}\right]^{\frac{1}{2}} \qquad (6)$$

and b is the Burgers vector of the dislocation, τ_c is the critical shear stress needed to propagate slip (taken to be $G/_{17}$), ν is Poissons ratio, G the bulk modulus and M_1, M_2 orientation factors. The term σ_o is known as the friction stress and includes terms such as the strength of a single crystal and hardening that results from increases in defect density (ρ). Since yield stress, σ_y, is related to hardness thus,

$$H = c\,\sigma_y \qquad (7)$$

[where c is the constraint factor and is expected to be 2-2.5 for ceramic materials such as TiN] then is it possible to interpret the "true" film hardness values derived from the volume law-of-mixtures hardness model using the Hall-Petch approach of equation (5).

For titanium nitride coating the increase in friction stress due to defect density can be approximated by[33]:

$$\Delta\sigma_\rho = 20.16 \times 10^{-6} \sqrt{\rho} \qquad (8)$$

and the grain size constant 'k' (equation 6) can be calculated as $1.16\ MN\ m^{-3/2}$. X-ray measurements allow determination of defect density[27], whilst TEM observations provide suitable estimates of grain size, and taking the hardness of a defect free single crystal as $1800\ kg\ mm^{-2}$[34] the friction stress contribution to total stress is

given by the term in parentheses below and the yield strength may be expressed thus:

$$\sigma_y = [7200 + 20.16 \times 10^{-6} \sqrt{\rho}] + 1.16\, d^{-\frac{1}{2}} \qquad (9)$$

Table 5 shows the various contributions to yield strength calculated for SIP-TiN on M2, SIP-TiN on austenitic stainless steel and compares these with estimates of the strength of a Balzers ion-plated TiN coating. From this simple analysis it is clear that grain size dominates the hardness of PVD coatings, the increase in hardness (yield strength) due to grain size being approximately an order of magnitude greater than that due to defects. Furthermore, the much finer grain sizes possible using ion-plating (by virtue of the high bias levels used) mean that these coatings are generally harder than SIP-TiN coatings. The experimentally determined hardness values for the SIP and ion-plated coatings are in good agreement with those calculated using the simple Hall-Petch approach and adequately accounts for the observed differences in hardness of the two types of coating. Thus, TiN coatings are hard principally due to their fine grain size.

4. CONCLUSIONS

The preceding sections have investigated the correlations that exist between bias, stress, hardness and microstructure and described the relevant structure-property relationships. Some general conclusions can now be drawn.

Increasing substrate bias serves to reduce grain size and densify the coating. By virtue of the denser microstructure, thermal stresses can now be supported and thus can contribute substantially to the internal stress. Hence, increases in substrate bias result in increases on both the intrinsic (growth) and thermal components of internal stress. The action of a large thermal stress may also promote further densification of the coating. Hardness is observed to increase with substrate bias and this has been attributed to refinement of grain size coupled with less porosity in the coating.

As SIP-coatings thicken, they are observed to become crystallographically textured, while the internal stress levels decrease and the porosity levels increase - grain size may also change. The hardness of thick coatings is found to be lower than thin coatings and this has been attributed to the increase in porosity toward the surface of the thicker coatings.

Hardness anisotropy has been observed in SIP-TiN and WTiC films and has been attributed to microstructural anisotropy coupled with changes in constraint (stress-state) associated with the preparation of metallographic cross-sections.

On nucleation, SIP-TiN coatings are found to have a {200} texture, however, during coating growth this tends toward a {111} texture as the favoured planes grow out into the vapour phase. The grain size of the SIP-TiN coating has been found to be sensitive to the nature of the substrate. Defects (probably dislocation loops) have been observed within the grains of SIP-TiN films and are thought to have been introduced by plastic yield of the film. No grain boundary or intra-granular [illegible]s have been found in our TiN studies.

The high hardness of PVD wear-resistant coatings (such as TiN) has been found to be principally dependent upon the fine grain sizes found in these coatings.

ACKNOWLEDGEMENTS

We wish to gratefully acknowledge financial support from the Department of Trade and Industry.

REFERENCES

1. W.D. Sproul and R. Rothstein, Thin Solid Films, 126 (1985) 257.
2. A.K. Chattopadhyay and A.B. Chattopadhyay, Wear, 80 (1982) 239.
3. P.A. Dearnley and E.M. Trent, Metals Technol., 9 (1982) 60.
4. R.A. Dugdale, Proc. Int. Conf. on Ion Plating and Allied Techniques, (CEP Consultants, Edinburgh, 1977), p. 177.
5. J.P. Coad and R.A. Dugdale, Proc. Int. Conf. on Ion Plating and Allied Techniques, (CEP Consultants, Edinburgh, 1979), p. 186.
6. A. Matthews and H. Sundquist, Engineering, (1983), Jan., p. 43.
7. J-E. Sundgren, Thin Solid Films, 128 (1985) 21.
8. J-E. Sundgren, B-O. Johansson, S-E. Karlsson and H.T.G. Hentzell, Thin Solid Films, 105 (1983) 367.
9. A. Matthews and D.G. Teer, Thin Solid Films, 73 (1980) 367.
10. M.K. Hibbs, B-O. Johansson, J-E. Sundgren and U. Helmersson, Thin Solid Films, 122 (1984) 115.
11. B.E. Jacobson, C.V. Deshpandey, M.J. Doerr, A.A. Karim and R.F. Bunshah, Thin Solid Films, 118 (1984) 285.
12. J.M. Poitevin, G. Lemperiere and J. Tardy, Thin Solid Films, 97 (1982) 69.
13. D.S. Rickerby, J. Vac. Sci. Technol. A, in press (1986); AERE Report R12204, 1986.
14. M.T. Laugier, Thin Solid Films, 117 (1984) 243.
15. L. Chollet, H. Boving and H.E. Hintermann, J. Mater. Energy Systems, 6 (1985) 293.
16. A. Aubert, J. Danroc, A. Gaucher and J.P. Terrat, Thin Solid Films, 126 (1985) 61.
17. B.A. Movchan and A.V. Demchishin, Phys. Met. Metallurgy, 28 (1969) 83.
18. J.A. Thornton, Ann. Rev. Mater. Sci., 7 (1977) 239.
19. J-E. Sundgren, B-O. Johansson and S.E. Karlsson, Thin Solid Films, 80 (1981) 77.
20. D.M. Mattox and G.J. Kominiak, J. Vac. Sci. Technol., 11 (1974) 671.
21. P.J. Burnett and D.S. Rickerby, Thin Solid Films, in press (1986).

22. P.J. Burnett and D.S. Rickerby, AERE Report R12232 (1986).

23. D.S. Rickerby and M.I. Wood, J. Vac. Sci. Technol. A, in press; AERE Report R12201 (1986).

24. P.M. Sargent and T.F. Page, Proc. Brit. Ceram. Soc., 26 (1978) 209.

25. D. Tabor, "The Hardness of Metals", Oxford University Press, Oxford, (1951) 105.

26. C.S. Barrett and T.B. Massalski, "Structure of Metals", McGraw-Hill, New York, 3rd Ed. (1966) p. 465.

27. D.S. Rickerby, B. Ballamy and A.M. Jones, in preparation.

28. L. Chollet and A.J. Perry, Thin Solid Films, 123 (1985) 223.

29. D.M. Marsh, Proc. Roy. Soc. Lond. A, 279 (1964) 420.

30. U. Helmersson, J.-E. Sundgren and J.E. Greene, J. Vac. Sci. Tech. A, 4 (1986) p. 500.

31. Y. Enomoto, Workshop on First Wall Coatings, Inst. of Plasma Physics, Nagaya Univ., Nov. 28-29, 1980. Eds. K. Kamada and M. Fukutomi, IPPJ-551, (1982), p. 202.

32. S. Vuorinem, E. Niemi and A.S. Korhonen, J. Vac. Sci. Technol A, 3 (1985) 2445.

33. R.M. Douthwaite, private communication.

34. H.J. Goldschmidt, Interstitial Alloys, Plenum Press, New York, 1967, p. 219.

Table 1 - Internal stress levels in PVD-TiN coatings

Process	Substrate	Thickness (μm)	Internal Stress (MPa)	Estimated Thermal Stress* at 500°C (MPa)
Sputter Ion Plating	Cemented carbide	6	+ 200	+ 1100
	Tool-steel (M2)	6	- 2100	- 1100
Ion Plating	Cemented carbide	2	- 4350	+ 1100
	Tool-steel (M2)	2	- 7400	- 1100
Ion Plating	Cemented carbide	11	- 1100	+ 1100
	Tool-steel (M2)	11	- 4450	- 1100

* As calculated using $\sigma_{th} \propto \frac{E_f \Delta\alpha \Delta T}{(1-\nu)}$

where $\Delta\alpha$ = difference between coating and substrate thermal expansion coefficients

ΔT = deposition temperature minus room temperature.

Table 2 - Best fit parameters for bias hardness modelling

Bias (V)	Thickness* (μm)	Substrate*			Film		
		$H_{10\ \mu m}$	M_s	E_s	$H_{10\ \mu m}$	M_f	E_f
0	1.7	210	1.9	200	800-1000	1.7-1.9	380
10	1.0 1.65	230 230	1.9 1.9	200 200	1900 1900	1.7 1.7	650 650
-35	1.2 2.0 4.8 5.5	190 180 180 180	1.9 1.95 1.95 1.9	200 200 200 200	2400 2400 2400 2400	1.7 1.7 1.7 1.7	600 600 600 600
-50	0.5 1.0	210 210	1.9 1.9	200 200	3200 3200	1.7 1.7	600 600

* Experimentally measured.

Table 3 - X-ray texture coefficients

Substrate	Thickness (μm)	T*		
		{200}	{111}	{220}
M2-tool steel	2 4 9	6.3 4.5 2.8	0.4 2.0 4.0	0.25 0.2 1.6
Austenitic stainless steel	1 2 5.5	6.6 5.0 4.4	0.3 1.3 3.1	0.2 0.4 2.85

$$T^*(h'k'l') = \frac{I_{h'k'l'}/I^o_{h'k'l'}}{1/n\ \Sigma_o^n\ (I_{hkl}/I^o_{hkl})}$$ where h'k'l' are the Miller indices of the plane of interest, I is a measured intensity and I^o a 'standard' intensity for a randomly oriented specimen. A value of unity corresponds to a random texture.

Table 4 - X-ray microstrain measurements (from ref. 27)

Substrate	Microstrain (%)		σ_{int} (MPa)
	Adherent	Free-standing	
M2	.18	.07	-2110
Martensitic - 420 stainless steel	.20	.14	-1500
Austenitic stainless steel	.24	.24	-4990

Table 5 - Estimated contributions of grain size and defect density to the hardness of PVD titanium nitride

System	Grain Size (Å)	Defect Density‡ (m^{-2})	Contribution to σ_y* ($MN\ m^{-2}$)			Calculated Hardness+ ($kg\ mm^{-2}$)	Observed Hardness $H_{10\mu m}$ ($kg\ mm^{-2}$)
			Single Crystal	Grain Size	Defect Density		
TiN or M2 by SIP, -35 V substrate bias	750 [TEM]	5.6×10^{13}	7200 (60.9)	4236 (35.8)	390 (3.3)	2957	2400
TiN on stainless steel by SIP	750 [TEM]	6.6×10^{14}	7200 (60.2)	4236 (35.4)	518 (4.4)	2989	2400
TiN on M2 by ion plating	200 [Estimate]	10^{16} [Upper bound estimate]	7200 (41.4)	8202 (47.1)	2010 (11.5)	4353	4500

‡ From X-ray Hall plots (see Ref. 27).
* Figures in brackets are percentage contributions to total σ_y.
+ Based on $H \approx 2.5\ \sigma_y$.

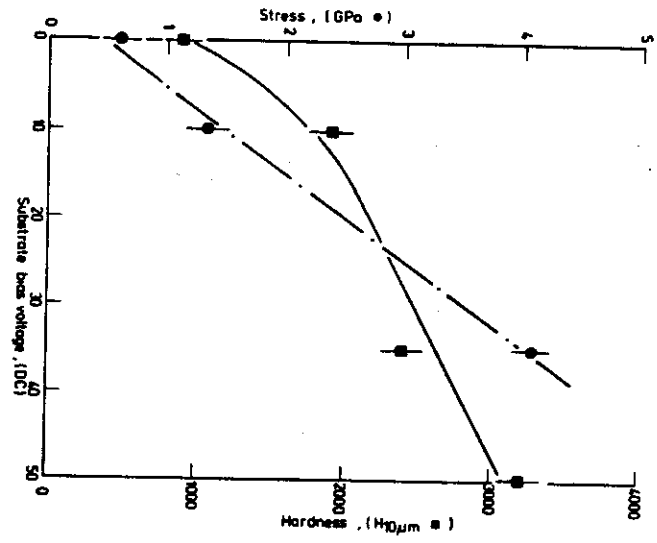

AERE R 12360 Fig. 1
The variation of compressive internal stress (●) and hardness ($H_{10\ \mu m}$ ■) with bias for sputter ion plated TiN onto stainless steel.

AERE R 12360 Fig. 2
Scanning electron fractographs (secondary electron image) of (a) unbiased and (b) biased titanium nitride coatings.

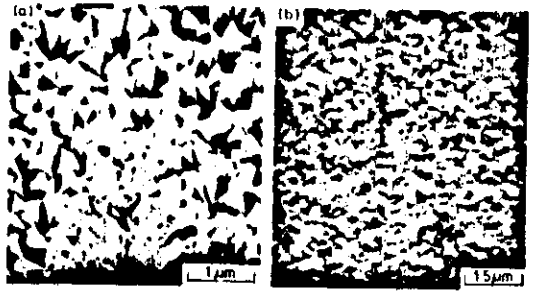

AERE R 12360 Fig. 3
Scanning electron micrographs of TiN coatings deposited with (a) no applied bias and (b) −35 V bias. Note the denser appearance of (b). The feature towards the bottom of (a) is the corner of a microhardness indentation.

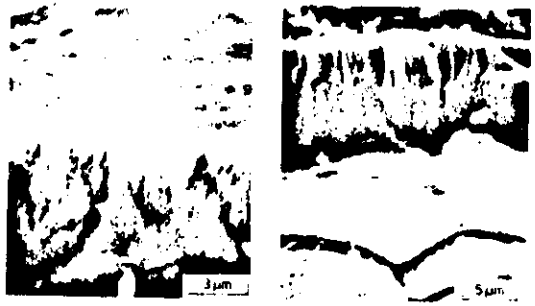

AERE R 12360 Fig. 4
Fracture surfaces of a tungsten-titanium carbide coating; left-hand micrograph for a coating adherent to a stainless steel substrate, right-hand micrograph of a free-standing section (scanning electron micrographs; secondary electron image).

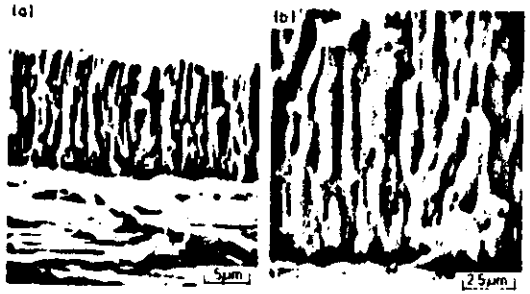

AERE R 12360 Fig. 5
SEM secondary electron image of fracture sections through SIP molybdenum coatings on a molybdenum substrate. (a) General view; (b) higher magnification showing open boundaries around the columns.

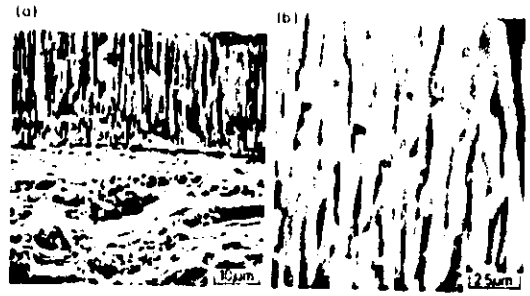

AERE R 12360 Fig. 6
SEM secondary electron image of fracture sections through SIP molybdenum coatings on a stainless steel substrate. (a) General view; (b) higher magnification. Note that the open columnar boundaries present in Figure 5 are now absent.

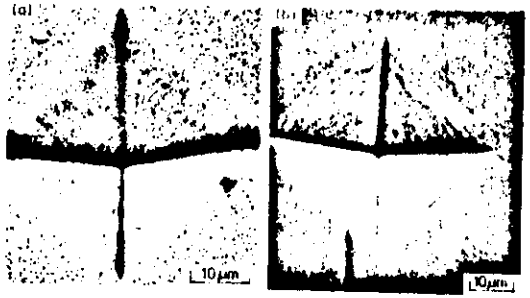

AERE R 12360 Fig. 7
SEM secondary electron image of 300 gf Vickers indentation on TiN coated stainless steel. (a) Unbiased; (b) −35 V bias.

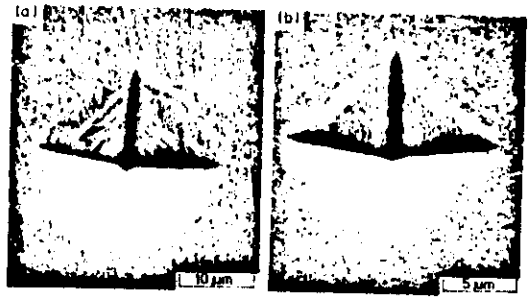

AERE R 12360 Fig. 8
SEM secondary electron images of 100 gf Vickers indentations on (a) TiN coated stainless steel (~5 μm) and (b) TiN coated M2 (~6 μm).

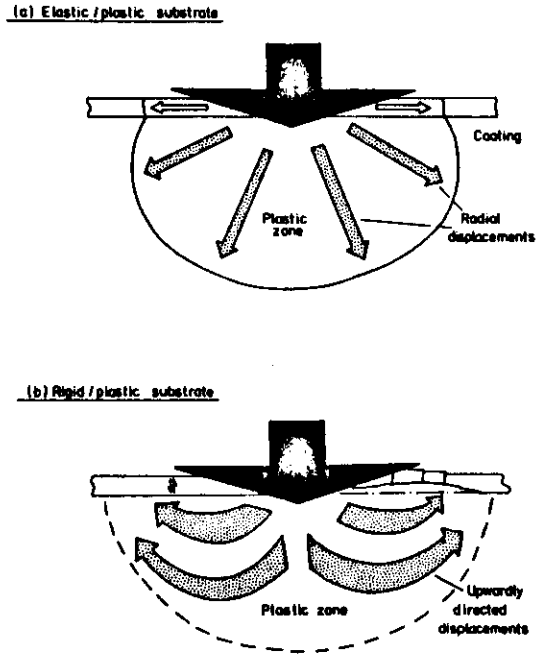

AERE R 12360 Fig. 9

A schematic representation of the deformation geometry beneath an indentation for (a) a hard coating on a hard elastic/plastic substrate, (b) a hard coating on a soft rigid/plastic substrate. Note the surface displacements in (b) that give rise to fracture of the coating.

AERE R 12360 Fig. 10

Pile-up of material around a 1 kgf indentation made on soft (rigid/plastic) stainless steel (reflected light micrograph, oblique illumination).

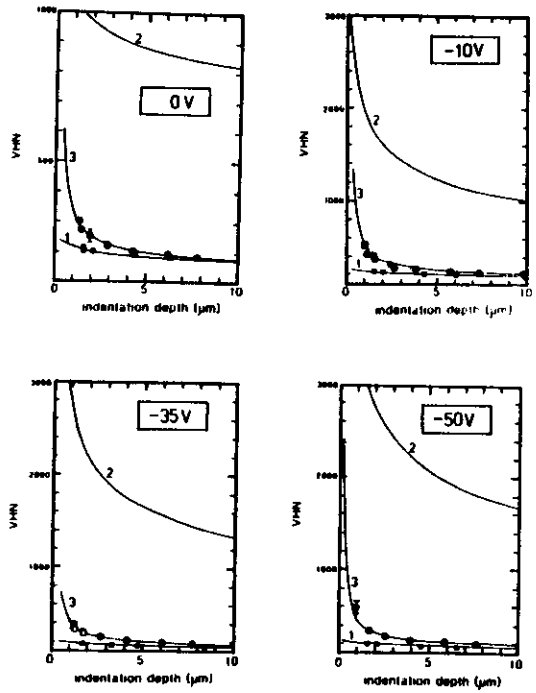

AERE R 12360 Fig. 11

Hardness vs. indentation depth plots for (a) 1.7 μm unbiased TiN, (b) 1.65 μm of TiN (−10 V bias), (c) 1.2μm of TiN (−35 V bias) and (d) 1 μm of TiN (−50 V bias) onto stainless steel substrates. The data points (● ○) are the experimentally determined composite hardness (open symbols representing measurements made from oblique illumination light micrographs), the data points (■) are measured substrate hardness values. Curves 1 are the substrate hardness behaviour assumed in subsequent calculations. Curves 2 are the "true" coating hardness behaviour assumed for calculation and curves 3 are the predicted hardness variation derived from curves 1 and 2 using the Burnett and Rickerby hardness model[21,22]. Good fits are achieved in all cases.

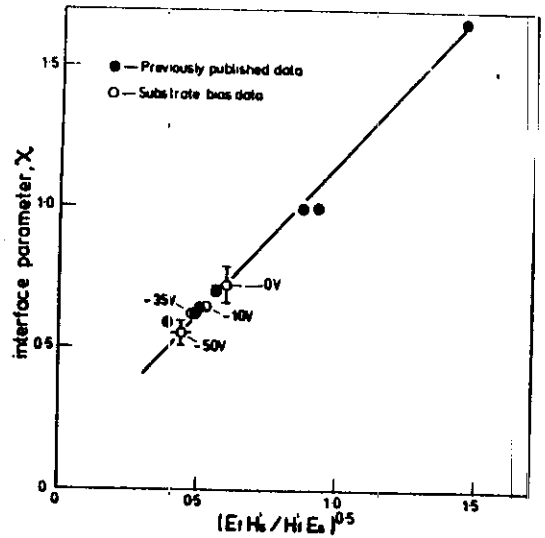

AERE R 12360 Fig. 12

Variation of the interface parameter χ vs. $(E_1H'_2/H'_1E_2)^{1/2}$ (the ratio of plastic zone sizes at a 100 μm indent size), used to obtain the fits in Figure 11. Note that all points are consistent with the trends from previous work.

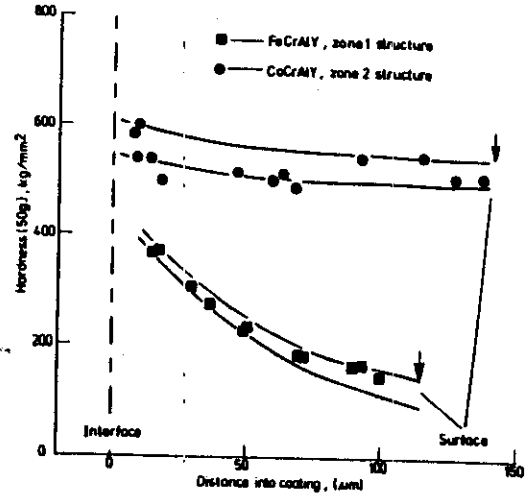

AERE R 12360 Fig. 13

The hardness (50 gf, Vickers) of FeCrAlY (■) and CoCrAlY (●) coatings as a function of distance from the coating/substrate interface obtained from indentation of metallographic cross-sections. Note that the Zone 1 structure of the FeCrAlY coating results in a softening towards the surface whilst the denser Zone 2 structure of the CoCrAlY coating results in an almost constant hardness.

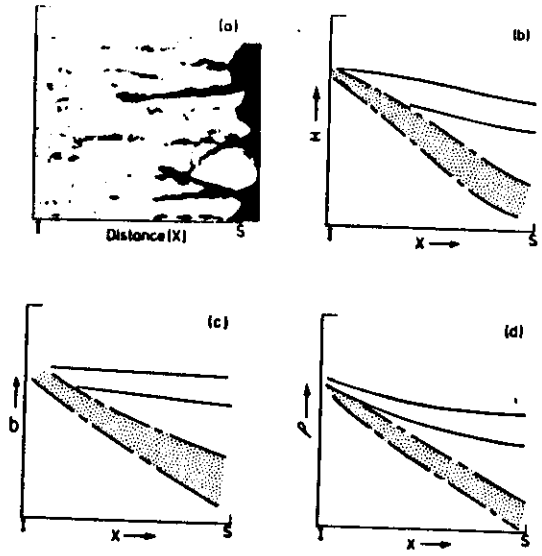

AERE R 12360 Fig. 14

(a) An etched metallographic cross-section of a FeCrAlY coating (similar to that used to obtain the hardness data for Figure 13) showing a Zone 1 type microstructure. Schematic variation of (b) hardness, (c) internal stress and (d) density with distance from the coating/substrate interface for Zone 1 microstructures (shaded bands) and Zone 2 microstructures (open bands). Note that for Zone 1 microstructures all three quantities decrease with distance whilst they are expected to remain approximately constant for Zone 2 microstructures.

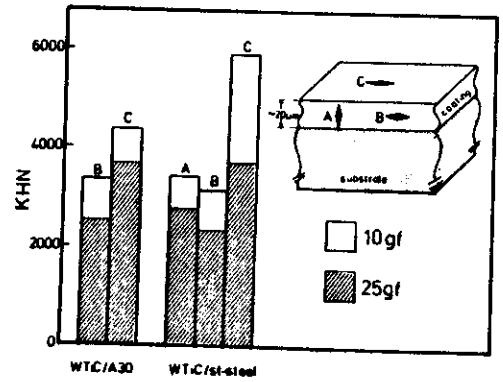

AERE R 12360 Fig. 15

The measured Knoop hardness values for a WTiC coating on A30 cemented carbide and austenitic stainless steel using three indenter orientations. Note the greater hardness of the orientation C in both cases.

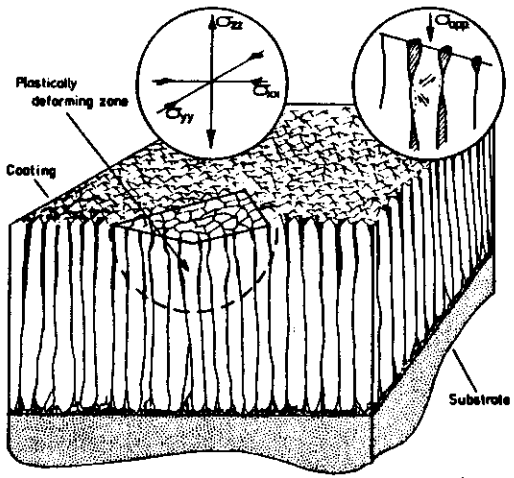

a

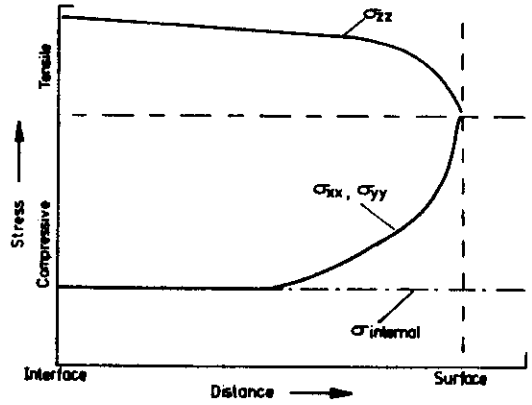

b

AERE R 12360 Fig. 16

(a) Schematic representation of the suggested deformation morphology of a PVD coating beneath a hardness indenter (orientation C in Figure 15). When indenting the columnar structural units "end-on" the columns expand and interact with their neighbours (see insert) once these interactions have occurred the neighbouring columns effectively constrain any further expansion. Thus, coatings with low levels of intercolumnar porosity will appear harder than those with high porosity. (b) A schematic representation of the stress-state acting in the coating shown in (a). Stress orientation as in insert in (a).

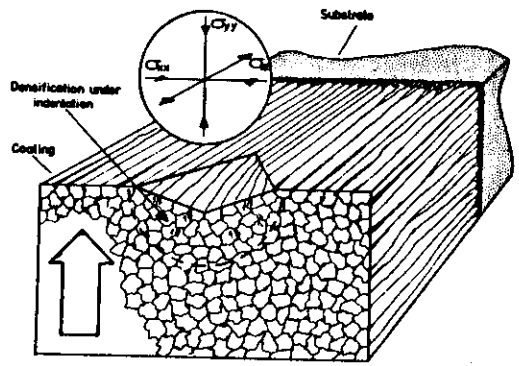

à

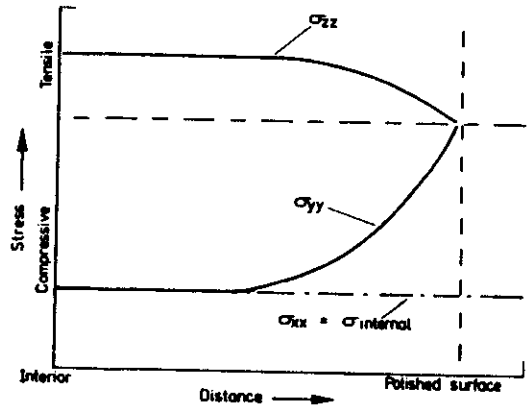

b

AERE R 12360 Fig. 17

(a) Schematic representation of the suggested deformation morphology of a PVD coating beneath a hardness indenter when indenting in cross-section (orientations A and B in Figure 15). Preparation of the cross-section releases the σ_{yy} compressive internal stress component close to the test surface (see (b)) which can result in the "opening up" of the columnar units towards the new surface (as indicated by the large shaded arrow). Indentation in this orientation can then result in densification of the columns together with sliding of the weak grain boundaries and buckling of the columns. This results in a low hardness compared to the "end-on" indentation of Figure 16.
(b) A schematic representation of the stress-state acting in the coating shown in (a). Stress orientation as in insert. Note that for a given depth into the coating the internal stress component σ_{yy} decreases towards the test surface whilst σ_{xx} remains relatively unaffected by the presence of the new free surface.

AERE R 12360 Fig. 18
Bright-field electron micrograph of a TiN film stripped from its M2-tool steel substrate.

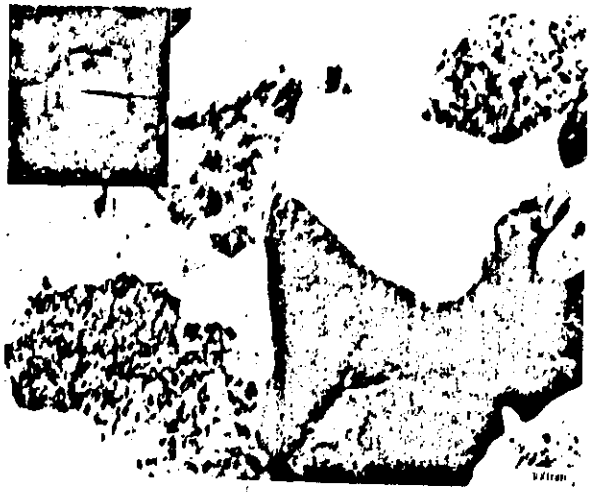

AERE R 12360 Fig. 19
Bright-field electron micrograph of a TiN film stripped from its martensitic-420 stainless steel substrate.

AERE R 12360 Fig. 20
Bright-field electron micrograph of a TiN film stripped from its austenitic stainless steel substrate.

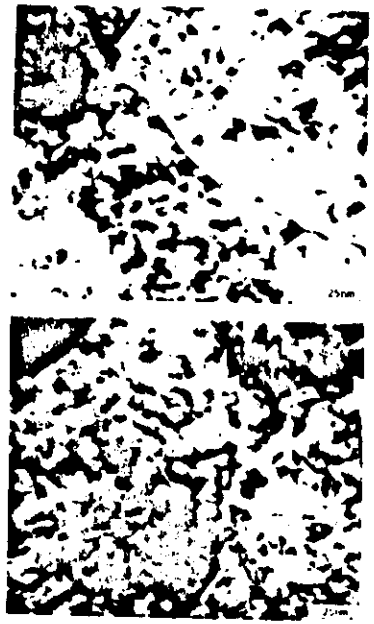

AERE R 12360 Fig. 21
Bright-field/dark-field pair of a region of TiN coating stripped from martensitic-420 stainless steel substrate showing a high density of defects thought to be dislocation loops.

Applications of ceramic films

I M BUCKLEY-GOLDER
Materials Engineering Centre, Harwell, Didcot, Oxfordshire

SYNOPSIS The use of ceramic films by the non-engine (gas turbine or reciprocating) industry is increasing worldwide in many applications e.g. in the electronics, wear, corrosion and optics fields. The main materials (e.g. SiO_2, Si_3N_4, TiN, Al_2O_3, ZrO_2, TiO_2, SiC) and processes (e.g. Physical Vapour Deposition, Chemical Vapour Deposition, Thermal Spraying) of interest are reviewed and examples of particularly useful non-engine applications are discussed to illustrate the factors to be considered when designing ceramic films in conjunction with components manufactured from different materials, e.g. metals, glass. General predictions are made to highlight the expected future developments in ceramic thin films.

1. INTRODUCTION

The resurgence of interest in ceramic materials for advanced technology applications is credited to the USA and Japan[1]. The potential use of bulk ceramics in engines has been the principal focus of popular interest over recent years. However, ceramic films (up to 2 mm thick) play an important role in engine developments but are also part of a much larger applications scenario in advanced technology and engineering with many important industrial consequences. For bulk ceramic materials, the Japanese have categorised this broader range of opportunities in terms of fundamental technical functions such as optical, nuclear, mechanical, biological, chemical and magnetic[2]. In this paper, the general opportunities for ceramic films will be addressed under these same headings, paying particular attention to non-engine applications.

2. MATERIALS FOR USE AS CERAMIC THIN FILMS

A number of ceramic materials are of interest for a range of thin film applications and include TiN, TiC, TiC/N, Si_3N_4, SiC, WC, Cr_2C_3, SiO_2, ZrO_2, Al_2O_3 and TiO_2. The oxides, nitrides and carbides tend to be of greatest applicability, but interest also exists in borides and sulphides for specific application areas e.g. TiB_2 for fusion reactor systems and ZnS for infra-red windows. A list of bulk ceramic properties is given in Table 1, but two points are worth noting regarding ceramic films: first, the properties of ceramic films can differ significantly from their bulk counterparts (e.g. the room temperature hardness of CVD Si_3N_4 can be ~ 20 GN/m^2 compared with 10 GN/m^2 for the bulk material[3]) and the Young's modulus of magnesia stabilised plasma sprayed ZrO_2 can be as low as 20 GPa compared to 200 GPa for bulk material[4]); and, secondly, the properties can be highly dependent upon the parent substrate which, if a metal, may yield to environment degradation, such as oxidation, before the ceramic film, thus causing coating failure by indirect rather than direct mechanisms. Attention to detail in the design of ceramic film-substrate combinations is thus very important.

Table 2 compares indicative values for representative properties of ceramics and metals[5-9]. The values have been chosen for bulk materials in each case as the properties of ceramic films are highly dependent upon processing routes. It is important to note that the ceramics and metals were also chosen as being typical of the materials which are of technological importance and which are often combined to produce a ceramic film on a metal, i.e. oxides, nitrides, carbides, iron, titanium, copper, and aluminium alloys. With the above provisos on detailed property values, the major property features of ceramic films may be summarised as follows:

- harder than metals
- better thermal insulators than metals
- in many cases electrical insulators
- generally of lower expansion coefficient than metals
- less environmentally sensitive than metals
- better in compression than tension.

Consequently, when seeking applications for ceramic films in terms of the technical functions highlighted in the Introduction, and when making preliminary design assessments, it is important to note the above distinguishing features.

3. SUMMARY OF PRINCIPAL THIN FILM DEPOSITION TECHNIQUES

Numerous techniques exist for the deposition of ceramic films onto components. Each technique is based on a phase conversion from either a liquid, vapour or solid to a thin film condensate which may or may not be fully dense. Examples of the main phase conversion processes are given below but it should be noted that many films can be deposited by more than one technique and that the deposition method can markedly affect the properties of the film as Table 3[10] shows for the example of Si_3N_4.

3.1 Liquid phase

Sol-gel technology, Figure 1, is a method of creating colloidal dispersions (sols) of ceramic particles (~ 200 Å in size) in a liquid matrix (organic or aqueous) and then using the sols either directly to form thin (~ 1-30 μm) washcoats on substrates which are subsequently calcined or, indirectly, by converting the sol to a gel powder (for example, by spray drying techniques) and then calcining the gel to form powders for plasma spraying.

3.2 Vapour phase

Chemical vapour deposition (CVD) relies upon thermally activating the chemical reaction of mixtures of gases at elevated temperatures (~ 700°-1100°C). Many thin films available commercially (e.g. TiC, TiN, Al_2O_3, Si_3N_4) are prepared by this technique. The technique is also useful as a means of infiltrating porous media and covering fibrous structures. Many substrates (e.g. iron alloys) will not withstand the temperatures involved without metallurgical degradation and therefore plasma activated/assisted vapour deposition (PAVD), as shown in Figure 2 to cover carbon fibres, may be used to lower the reaction temperatures to a level where substrate damage is minimised. For example, the deposition of SiC by CVD normally occurs at 1000-1600°C, but the PAVD mode has been shown to lower the reaction temperature to ~ 250°C and allow brass to be successfully treated[11].

3.3 Solid to vapour phase conversion

Two principal processes fall under this heading: electron beam evaporation and sputtering which are shown schematically in Figure 3(a) and 3(b) respectively. In the former case, the thin film material (e.g. ZrO_2) is vaporised under high vacuum (10^{-6} Torr) conditions by an electron beam (lasers and resistance heating could also be used) the vapour then depositing onto the substrate of interest. In the latter case, the surface of the thin film source material is sputtered under vacuum conditions (10^{-3}-10^{-6} Torr) by bombardment with a heavy inert gas atom (e.g. Ar) and diffuses to the substrate.

In both cases, although thin films have been deposited using the original ceramic as the source material, the preferred route is often to use metal (e.g. Al, Zr, Si) as the source material which is then reactively combined in a partial pressure of the appropriate gas (e.g. O_2/N_2) to yield the preferred ceramic (e.g. Al_2O_3, Si_3N_4, ZrO_2) film.

Compositional control is thus made easier and the risks of source material degradation (e.g. thermal stress cracking) are reduced. Plasmas may also be used to activate/assist the vapour phase reactions.

3.4 Solid to liquid phase conversion

Thermal spraying technologies (Figure 3(c) shows an example known as plasma spraying) rely upon the conversion of powders to liquid droplets in a suitable heat source (e.g. oxy-acetylene flame, plasma gun) and projecting the droplets at high velocity (100-800 m/s depending upon the technology) onto a substrate where rapid fusion (~ 10^4-10^5 K/s) occurs yielding a ceramic film made from individual "splatted" droplets. Thus, providing the flame can impart enough heat to the powder particles to cause melting (hence the advent of high temperature plasmas operating at 10,000-15,000°K) and the powders will undergo melting, spraying technologies are capable of depositing a wide variety of ceramic materials under atmospheric or soft vacuum conditions.

3.5 General considerations when comparing coating techniques

It is important to note a number of general points when comparing coating techniques:

- vacuum chambers limit the size of component which can be processed
- vacuum processing often requires sophisticated component handling during deposition to ensure uniform coverage around complex geometries e.g. drills, cutting inserts and valves
- vacuum processing confers the distinct advantage of in-situ component cleaning e.g. by sputter cleaning, which greatly assists thin film to substrate bonding
- if thin film purity is important, then vacuum chambers should be dedicated to specific compositions as cross contamination may occur
- plasmas are increasingly important for all types of ceramic deposition except the preparation of thin film wash coats by sol-gel technology
- coupling spraying technologies with robotic processing considerably extends their scope
- atmospheric processing techniques (i.e. sol-gel and spraying) offer the potential for providing relatively simple ceramic films off-site; other techniques require centralised processing facilities.

4. APPLICATIONS OF CERAMIC FILMS

The applications of ceramic films are extensive. Within an overview of this kind, only examples of applications will be reviewed to demonstrate particular points of importance using the Japanese classification of technical functions as a guideline.

4.1 Chemical

Work is presently underway[12] into the use of PAVD to produce thin (~ 5 μm) SiO_2 layers on alloys of interest to the advanced heat exchanger industry (high alloy steels) to combat oxidative and corrosive attack at elevated temperatures. It has been demonstrated that SiO_2 layers can reduce carburisation by a factor of 8 after exposure to 1050°C for 500 hours. This work is also an interesting example of the way in which more than one deposition technique may be useful: originally, both sol-gel technology and PAVD were viewed as offering the potential to contribute to the solution of the problem of chemical attack on heat exchangers. Parallel, detailed work on both systems showed an eventual preference for PAVD as

being able to offer adherent, dense coatings on relatively complex geometries. Moreover, post deposition processing such as laser surface modifications has been shown to improve the corrosion resistance.

Although ceramic films may be used for surface protection and/or insulation they may also be used with considerable promise as gas sensitive surface layers. For example, it has been shown that sol-gel technology can be used to provide thin (~ 3 μm) films of Al_2O_3[13] on ceramic substrates supporting thick film electronic circuitry or CeO_2/SiO_2[14] on wire mesh used as a catalyst substrate. In the latter case, the ceramic film acted as a high surface area, porous medium for subsequent incorporation of catalytically active species (e.g. Pt) in exhaust gas modification work (Figure 4), whilst in the former example, the sensitivity of the porous ceramic film to environmental moisture realised a range of humidity sensing devices by monitoring the electrical resistance change of the film as a function of humidity, Figure 5.

4.2 Optical

Optical thin films are required in a range of industries such as energy conversion (solar cells), building (architectural glass) and automotive (mirrors) to modify the ways in which electromagnetic radiation in the visible and infra-red regions of the spectrum is absorbed and/or reflected. Even very thin layers (~ 500 Å) can have a marked effect, as shown in Figure 6(a). After much fundamental work, an industrial preference was found for sputtering techniques, which enabled high quality (dense, adherent, controlled composition) films of TiO_2 and Al_2O_3 to be deposited satisfactorily[15]. Moreover, once the basic deposition requirements had been satisfied it became a natural step to deposit multilayer films of TiO_2-Ag-TiO_2 and TiO_2-Cu-TiO_2 to provide controlled i.r. reflectance surfaces. Industrial user acceptability depended upon detailed analyses of environmental response since ingress of oxygen through the outer layer of TiO_2 could cause oxidation of the Ag/Cu. A solution was found in the use of a fourth layer of unspecified composition. Fundamental work such as this has culminated in the installation of advanced vacuum deposition plant for architectural glass (e.g. in the USA, UK and Sweden) where the economics of operation require a high throughput of glass (~ 0.1-1 x $10^6 m^2$/year), which, in turn, demands semi-continuous processing, as shown schematically in Figure 6(b). In the most modern plant, a slab of glass measuring 6 m x 2.5 m emanates every 2 minutes after having received four sputtered films, at least two of which are ceramic.

4.3 Mechanical

Wear resistance is a major application area dependant on mechanical properties. A range of ceramic films are now available commercially such as TiN, TiC, Al_2O_3 and WC deposited by various methods including PVD, CVD and spraying. In each case success has depended upon extensive fundamental work into process and materials science combined with industrial evaluation. The more instructive examples are summarised below:

- 1-3 μm films of TiN deposited by PVD (sputtering and evaporation) and CVD onto cutting tools (e.g. drills, taps) have been shown to reduce cutting wear and increase tool life by up to x10. The high hardness and low friction of TiN are thought to contribute to the success. In production machines approximately 1500 drills can be coated in one batch[16]. An important trend is towards developing low temperature (< 300°C) processes to enable temperature sensitive substrates (e.g. aluminium alloys, low alloy steels) to be coated. Additionally, alternative material compositions are proving to be of value in the attempt to improve upon the acknowledged performance of TiN, e.g. WC, Cr_2C_3.

- CVD multilayer ceramic films of TiC-Al_2O_3-TiN on indexable carbide inserts have dramatically enhanced the performance of the insert to the extent that cutting speeds of 400 m/min are not uncommon. This was achieved through an understanding of the detailed tool-workpiece cutting environment and recognising that tool degradation mechanisms varied around the tool. Hence, TiC is used to resist abrasive and attrition wear on the tool flank; Al_2O_3 is resistant to dissolution in iron alloys at the local cutting temperature of 1000°C and TiN both reduces friction and makes the tool more identifiable (being golden in colour) from a marketing viewpoint[17].

- Spraying technologies have been used to manufacture artefacts of ceramics e.g. ZrO_2, Al_2O_3 where deposition onto a disposable mandrel allows near nett shapes to be fabricated. Examples include crucibles and power coil tubes[18].

- PAVD is regularly used to deposit GeO_2 doped SiO_2 onto the inside of a SiO_2 tube which is then thermally collapsed to provide a duplex material containing a SiO_2 doped core and a SiO_2 sheath. The composite cylinder is then used as the source material for drawing many km of optical fibre[19].

4.4 Electronic

Ceramic films (SiO_2, Si_3N_4) 250 Å-1 μm thick are regularly deposited in the electronics industry as insulating layers in the fabrication of semiconductor devices. The coating techniques used include PVD, CVD and PAVD. At this scale, the smallest surface defect (dust, crack, pore) on the substrate is either replicated in the topography of the film, or, causes defects in the film (e.g. discontinuous coverage) irrespective of whether it is ceramic or not. Figure 7 summarises the type and size of defects which are of particular concern. In passing it is also important to note the type of techniques necessary to interrogate the microstructure of very thin films i.e. mainly electro-optical.

It has thus proved necessary to adopt advanced processing environments where cleanliness is important. Cleanliness is increasing in importance to the extent that future facilities will probably eliminate process operators and be undertaken in-vacuo by remote control. In the USA the establishment of a Microcleanliness Unit to serve the industry demonstrates this current trend. Advanced diagnostics such as laser fluorescence are also proving necessary to monitor environmental quality.

4.5 Magnetic

In the data/information storage media industry the trend is towards using thin film deposition techniques (principally PVD sputtering) to lay down a magnetic film with a vertical preferred orientation[20]. By controlling the microstructure during sputtering, as shown schematically in Figure 8, it is possible to grow fine columnar grains perpendicular to the substrate plane. Each grain then becomes a small magnetic domain which can change sign (NS or SN) by the application of an external magnetic field from a small geometry magnetic pole-piece. Packing density increases of x10 have been achieved as a result. γ-Fe_2O_3 has been examined for this application together with Co-Cr alloys[21]. This particular use for sputtering again demonstrates the need to control thin film characteristics in detail in order to achieve success.

4.6 Biological

Experimental work is underway to examine the potential for ceramic films in biological environments. The main application is as a wear resistant coating on prosthetic hip joints, especially as a covering on the ball. Data from Al_2O_3-TiO_2, Al_2O_3 and SiC deposited by spraying and PAVD indicate that wear rates can be dramatically reduced[22]. However, further extensive work is required to assess reliability from a biocompatibility viewpoint. Technical and commercial competition from ion implantation into metals and bulk ceramic joints will also be intense and may not augur well for the future of wear resistant ceramic films in humans.

4.7 Nuclear

In the nuclear industry ceramic films are of potential importance for advanced gas cooled reactors (AGR's) to minimise carbon deposition on the surface of fuel cans, which adversely affects heat transfer and operating efficiency, and to improve the oxidation resistance of the fuel can material to allow higher temperatures of operation. Considerable R&D has been undertaken on the deposition of SiO_2 films on AGR fuel elements by CVD and PAVD techniques and these have given effective protection in laboratory evaluations[23].

5. FUTURE TRENDS AND CONCLUSIONS

From the information presented here a number of trends and conclusions are drawn as follows.

- The requirement to design with ceramic films will grow in importance to meet end users' requirements for gains in performance.

- The detailed characterisation and properties of ceramic films are poorly understood and much work remains to be done.

- Many advanced developments will depend on extensive fundamental work.

- The characterisation of ceramic films is an area of especial importance and requires detailed work in conjunction with process technology.

- Automated/robotic processing will lead to increased reliability, reproducibility and to reduced processing costs.

- Plasma technologies will play an increasing part in ceramic film development.

- Clean room processing will grow in importance for very advanced thin film (< 1 μm) applications.

- For machining and wear applications, new compositions and lower deposition temperatures are important lines of development.

6. ACKNOWLEDGEMENTS

The author acknowledges the help of numerous colleagues at Harwell and elsewhere in the preparation of this overview.

REFERENCES

(1) Ceramic Industry, May, 1984, p. 22.

(2) KERNAY, G.B. and BOWEN, K.H., Am. Cer. Soc. Bull., 1983, 62, no. 5, 590.

(3) NIIHARA, K. and HIRAI, T., Power Metallurgy International, 1984, 16, no. 5, 223.

(4) WELLS, J.D., BUCKLEY-GOLDER, I.M. and SCOTT, K.T., Harwell, Unpublished Work.

(5) SMITHELLS, C.J., Metals Reference Book, 5th Edition, 1976.

(6) SAMSONOV, G.V., The Oxide Handbook, IFI/Plenum, New York, 1973.

(7) Engineering Property Data on Selected Ceramics, Battelle Columbus Laboratories: Vol. I - Nitrides, 1976; Vol. II - Carbides, 1979; Vol. III - Single Oxides, 1981.

(8) WOOLMAN, J. and MOTTRAM, R.A., The Mechanical and Physical Properties of the British Standard En Steels, Vol. 1-3, The British Iron and Steel Research Association, Publ. Pergamon Press, 1969.

(9) COOTHER, M.K.R. and HODGSON, P., Trans. J. Br. Ceram. Soc., 1982, 89, 141.

(10) MORASANU, C-E., Thin Solid Films, 1980, 65, 171.

(11) COAD, J.P. and AYRES, C., Harwell, Unpublished Work.

(12) NPL Report, DMA(D)484, April, 1985.

(13) McGEEHIN, P., WILLIAMS, D.E. and TOFIELD, B.C., UK Patent Appl. No. 2 138 321A, 1984.

(14) NELSON, R.L. et al, Thin Solid Films, 1981, 81, 329.

(15) LEYBOLD-HERAUS, UK Patent Appl. GB 2134741A, 1985.

(16) MATHEWS, A., Surface Engineering, 1985, 1, 93.

(17) JACK, D.H., I. Mech. E. Conf., Applications of Engineering Ceramics, 26th February, 1986.

(18) SCOTT, K.T., Harwell, Unpublished Work.

(19) GEC, Hirst Research Centre, Private Communication.

(20) IWASAKI, S., Transactions on Magnetics, IEEE, 1984, Vol. Mag-20, no. 5, 657.

(21) ESPRIT II Planning Meeting, February, 1986.

(22) DOWSON, Prof. D., I. Mech. E. Conf., Applications of Engineering Ceramics, 26th February, 1986.

(23) CAIRNS, J.A. et al, Nature, 1980, 288, no. 5792, 686.

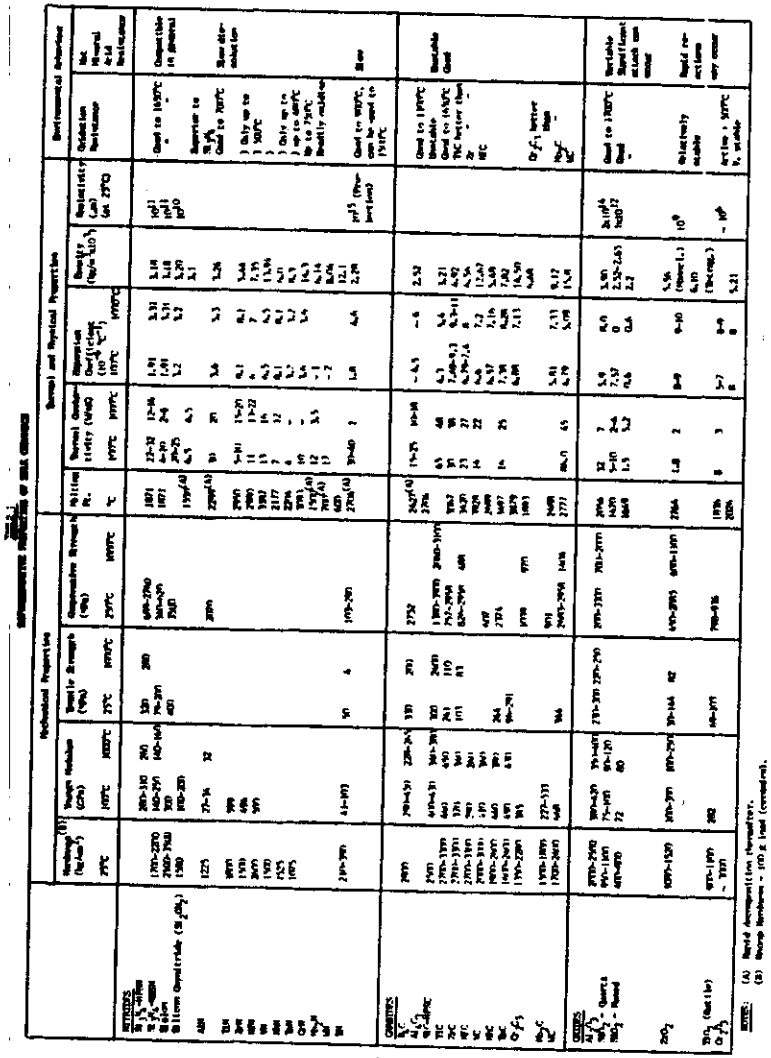

TABLE 2

A STRAIGHTFORWARD COMPARISON OF THE REPRESENTATIVE PROPERTIES OF BULK CERAMICS AND METALS

Property	Performance Advantage	Typical Ratio*
Hardness	Ceramics > Metals	: 3:1
Density	Metals > Ceramics	1.6:1
Melting Point	Ceramics > Metals	2:1
Thermal Conductivity	Ceramics < Metals (exceptions e.g. SiC, TiC)	1:6.0
Thermal Expansion	Metals > Ceramics (exceptions e.g. ZrO_2)	.3:1
[illegible]	Metals < Ceramics	1:1b[18]
Mechanical Properties	Metals < Ceramics - Compression Metals > Ceramics - Tension	1:2.5 .3:1
Environmental Behaviour	Ceramics > Metals	

*Based on oxide, nitride and carbide ceramics and iron, aluminium, copper and titanium alloys.

TABLE 3

TYPICAL PROPERTIES OF Si_3N_4 FILMS

Preparation Method	Density ($g\ cm^{-3}$)	Refractive Index	IR Absorption Maximum	Dielectric Constant	Electrical Resistivity (Ω cm)	Dielectric Strength (10^6 V cm^{-1})	Etch rate (A min^{-1})		
							HF	1:10 HF:NH_4F	H_3PO_4
CVD, SiH_4+NH_3	2.75-3.11	1.9-2.7	11.7	6-8.7	1×10^{14}	5-10	90	5	60
CVD, $SiCl_4$+NH_3	3.1	2.0-2.8	11.7	4.8-5.8	1×10^{14}	10	-	11	100
CVD, SiH_4+N_2H_4	3-3.1	2.0-2.1	11.3	6.1	1×10^{14}	6-10	300	-	-
CVD, SiH_2Cl_2+NH_3	-	1.9-2.1	11.5	5-9	1.5×10^{14}	10	600	150	75
RFGD, SiH_4+NH_3	-	1.9-2.8	12.1	7-11	8×10^{16}			50	
RFGD, SiH_4+N_2	-	2-2.5	12	4-7	-	1		100	
LPCVD, SiH_4+NH_3	-	1.98-2.08	-	-	-	5-10	150		
LPCVD, SiH_2Cl_2+NH_3	-	2.00	-	-	-	-	200		
Direct r.f. sputtering	3	1.9-2.08	-	-	-	-	750		
Reactive r.f. sputtering	2.8-3	2-2.1	-	6.2-6.8	-	0.2-7			
CVD $Si_xO_yN_z$	2.1-3.1	1.44-2.03	9.2-11.7	3.9-7.4	-	10	>360	>600	>600

CVD = chemical vapour deposition
RFGD = radio frequency glow discharge
LPCVD = low pressure CVD

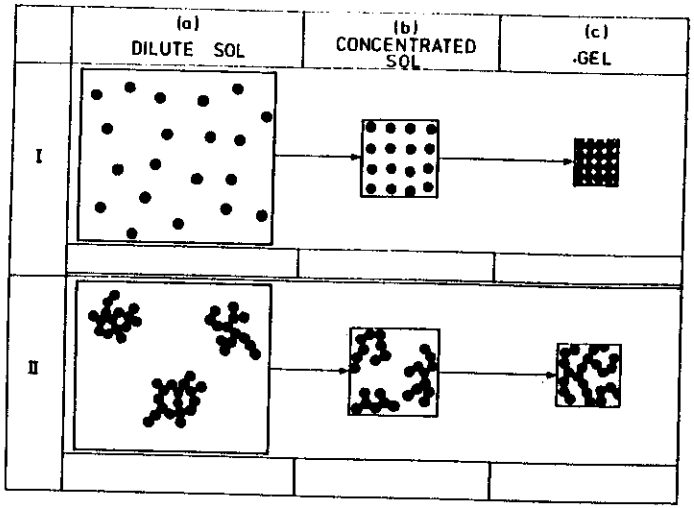

Fig 1 Diagram illustrating the formation of gels of low and high porosity from (I) unaggregated and (II) aggregated sold, respectively

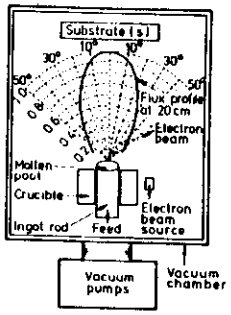

Fig 3(a)

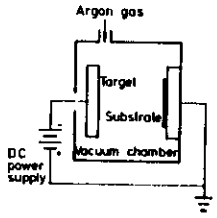

Fig 3(b)

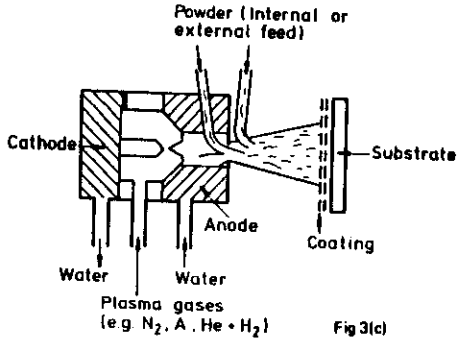

Fig 3(c)

PLASMA-ACTIVATED VAPOUR DEPOSITION (P.A.V.D)

β-Silicon carbide coatings on 10.000 filament carbon tows.

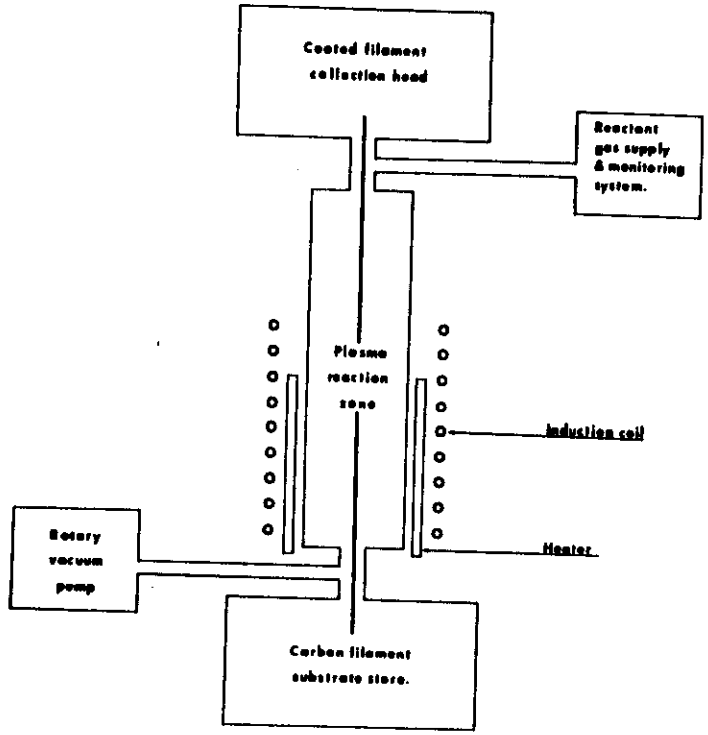

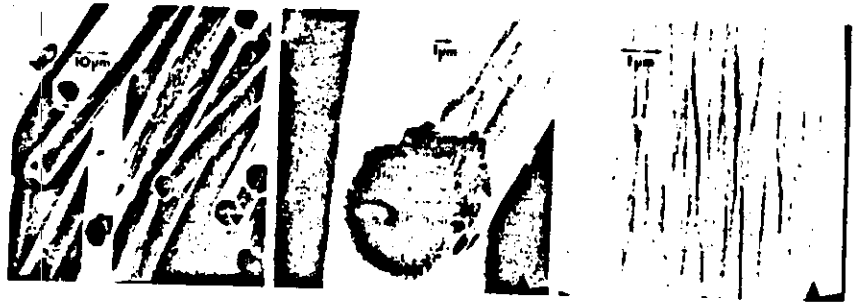

Fig 2 Plasma-activated vapour deposition (PAVD). β-silicon carbide coatings on 10 000 filament carbon tows

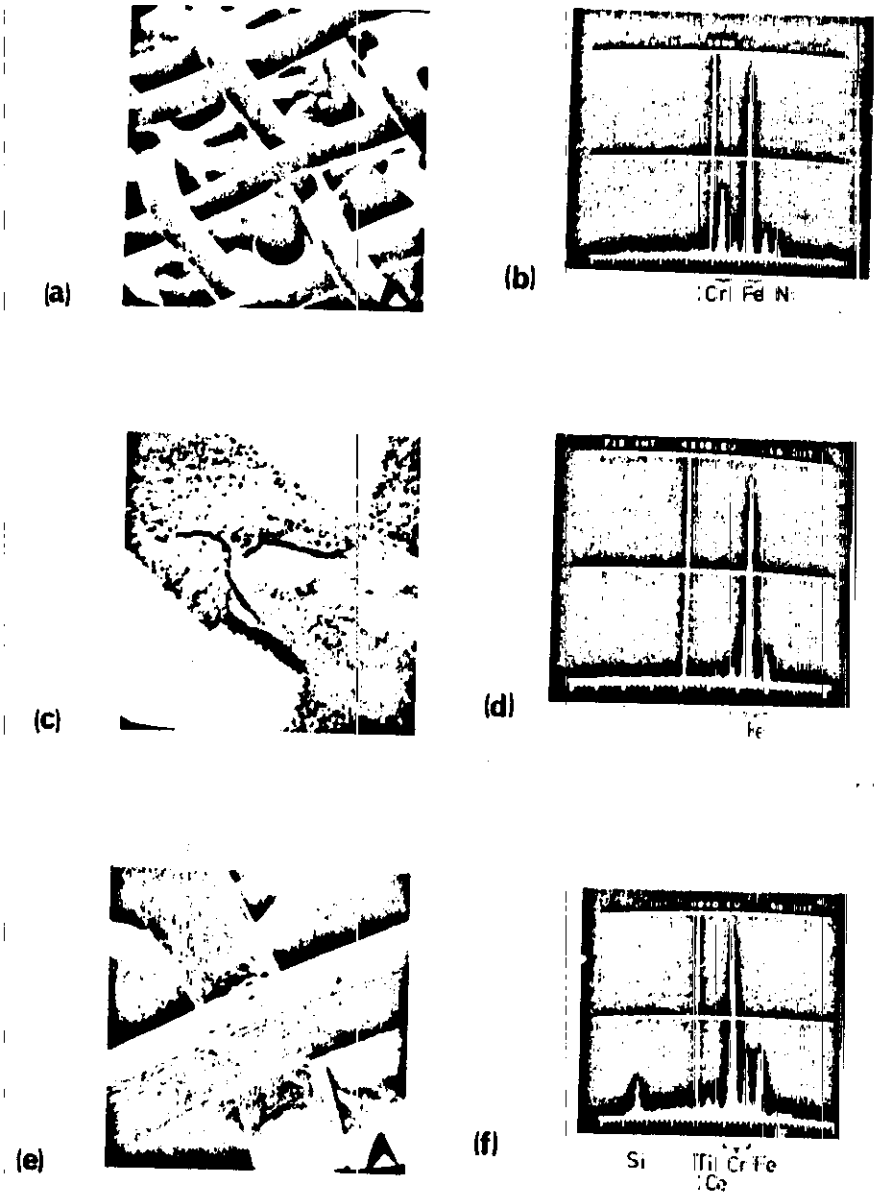

Fig 4

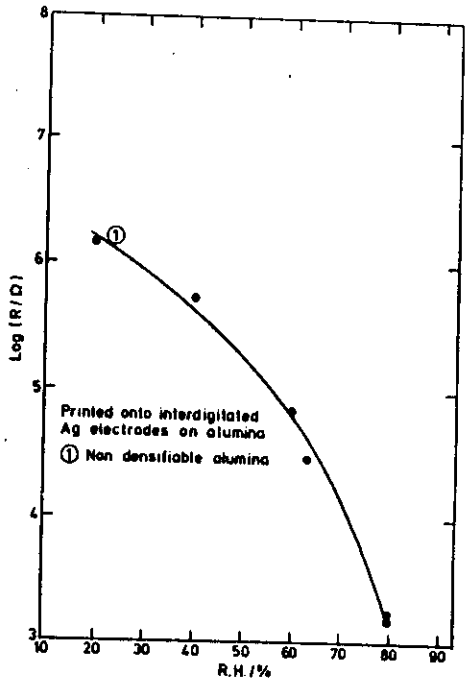

Fig 5 Humidity response of prototype devices at 20°C

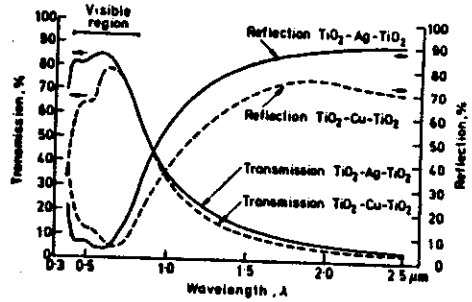

Fig 6(a) Transmission and reflection versus wavelength between 0.38 and 2.6 μm for the following multilayer systems: —— TiO_2 (30nm)/Ag (13 nm) /TiO_2 (36nm); - - - TiO_2 (30nm)/Cu (13nm) /TiO_2 (36nm)

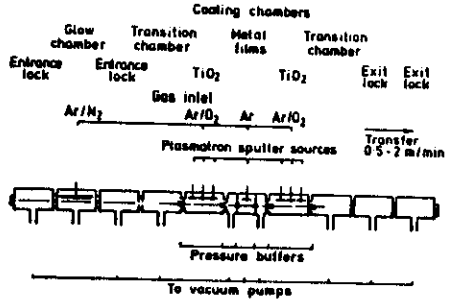

Fig 6(b)

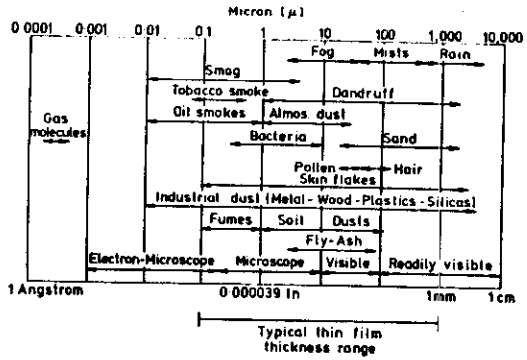

Fig 7

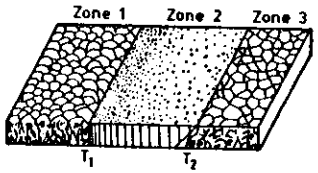

	Zone 1	Zone 2	Zone 3
Metals	$<0{\cdot}3\,T_m$	$0{\cdot}3-0{\cdot}45\,T_m$	$>0{\cdot}45\,T_m$
Oxides	$<0{\cdot}26\,T_m$	$0{\cdot}26-0{\cdot}45\,T_m$	$>0{\cdot}45\,T_m$

Fig 8(a) Structural zones in condensates at various substrate temperatures, after Movchan and Demchishin

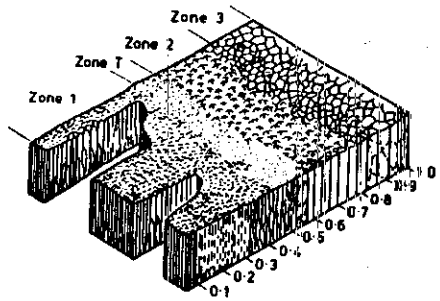

Fig 8(b) Structural zones in condensates showing the effect of gas pressure, after Thornton

STRUCTURE, PROPERTIES AND APPLICATION OF TITANIUM NITRIDE COATINGS PRODUCED BY SPUTTER ION PLATING

D.S. Rickerby* and R.B. Newbery+

ABSTRACT

The potential beneficial effects that wear-resistant coatings have on engineering surfaces depends upon their ability to remain adherent with the treated component. This paper concentrates on the process of sputter ion plating, a simple D.C. glow discharge sputtering system operating in soft vacuum, and relates the properties of titanium nitride coatings to the degree of ion polishing (substrate bias) which is utilised during deposition. Substrate bias was identified as the most important system's parameter since it allowed for some stress relaxation within the coating via its influence on porosity levels in the coating microstructure. The influence that this has on coating adhesion is discussed. The internal stress is a combination of intrinsic growth stresses and thermal mismatch stresses with the latter tending to dominate as substrate bias is increased. In addition to substrate bias, the role that titanium interlayers and substrate cleaning play in improving the adhesion of titanium nitride coatings is discussed, and the potential benefits highlighted. In the last part of the paper some applications of titanium nitride coating are described - it will be shown that increase in component life is by no means the only criterion which should be considered when judging the success, or otherwise, of a coated component.

INTRODUCTION

Physical vapour deposition (PVD) coating processes are capable of producing hard wear-resistant surfaces on cutting tools below their softening or tempering temperatures. At present the most popular coating is titanium nitride. To optimise performance it is important to understand the inter-relationship between the structure of the coating and its properties. The level of coating/substrate adhesion is of particular importance and is generally measured in these well-bonded titanium nitride coatings by means of the scratch test (ref 1). One of the most important factors which influences the adhesion of these hard wear- resistant coatings is the level of internal stress present in the coating which can be manipulated by application of a substrate bias (refs 2, 3). The purpose of this paper is to outline the salient features of sputter ion plating (SIP), a simple glow discharge sputtering system which has been developed in a joint venture between Harwell and TI. The use of substrate pre-treatments to improve the adherence of the titanium nitride coatings is discussed and the role of the parameter 'substrate bias' in determining not only the composition of the coating but also its physical properties and microstructure is considered (refs 3,4). The paper goes on to illustrate the engineering benefits of SIP TiN coatings with examples which include cutting, slitting, bearing and anti-seizure applications.

*Materials Development Division, Harwell Laboratory, UKAEA, Harwell, Didcot, Oxfordshire OX11 ORA.
+TI Research, Hinxton, Saffron Walden, Essex CB10 1RH.

THE USE OF CLEANING PRE-TREATMENTS IN PVD PROCESSES

In a number of the PVD processes, a variety of pre-treatments have been employed to ensure good adhesion of the titanium nitride coating. This section of the paper reviews these pre-treatments with particular reference to sputter ion plating (SIP, refs 5,6). In the SIP process, titanium atoms are sputtered from source cathodes and react in a low partial pressure of nitrogen to form titanium nitride at the surface of the components. A substrate bias applied during growth promotes 'ion-polishing' of the deposit and this ensures a dense coating microstructure (ref 7); see also ref 2 for further details.

The first pre-treatment to consider is sputter cleaning or ion-bombardment of the workload. This is accomplished by applying a large negative voltage (500-1000 V) on the samples, causing sputtering of the surface by argon ions. In the case of SIP, this stage is preceded by pretreating to 300°C to break down any carbonaceous residues which may be on the surface and to desorb any loosely-bonded material (ref 8). The principal role of ion cleaning is to remove friable oxide layers on the surface of metals. Fig.1 shows the variation in the critical load for coating loss (L_c), as measured by a scratch test, with pre-treatment ion- clean voltage for titanium nitride deposited onto polished stainless steel coupons. Similar observations have been reported for tool steel substrates by Helmersson et al. who also considered the role of substrate temperature (ref 9).

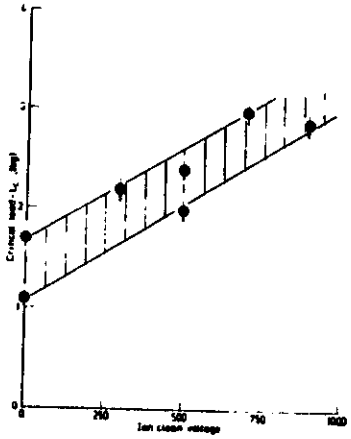

Fig. 1 Variation of critical load (L_c) with ion clean voltage for titanium nitride coatings deposited onto stainless steel

These improvements in coating/substrate adhesion which result from ion cleaning are clearly shown in fig.2 which compares the scratch tracks at a load of 15 N for surfaces without and with sputter cleaning (figs.2(a) and 2(b) respectively). For an ion cleaned substrate, only conformal cracking is observed along the edge of the scratch track whilst flaking (localised coating loss) is readily apparent for titanium nitride coatings deposited onto substrates without a sputter cleaning stage (fig.2(a)).

In addition to ion or sputter cleaning, to enhance the adherence of the coatings a thin interfacial layer of pure titanium is deposited prior to forming the nitride. Fig.3 shows the variation in critical load for coating loss (L_c) with titanium sputter time (i.e. interlayer thickness) for sputter ion plated titanium

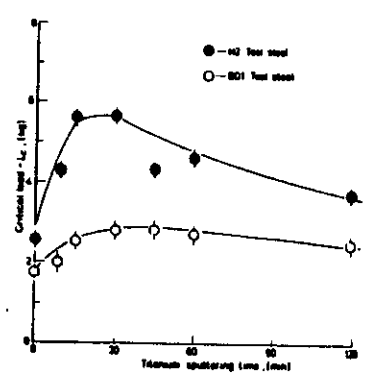

Fig. 3 Variation of critical load (L_c) with titanium sputtering time (interlayer thickness) for TiN coatings onto ferritic steels

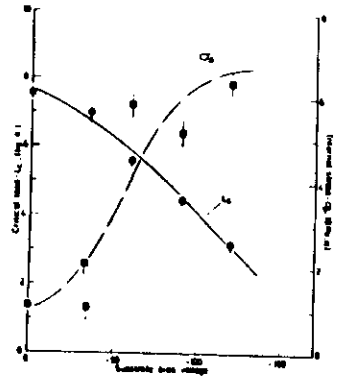

Fig. 4 The variation of compressive internal stress (■) and critical load (•) with bias for sputter ion plated TiN onto M2 tool steel

nitride coatings deposited onto two ferritic steels at a temperature of approximately 500°C. Clearly, for both coating/substrate combinations there is an optimum titanium interlayer thickness, and the peak adherence occurs at a titanium sputtering time of 30-40 mins which is equivalent to 0.1-0.15 μm of titanium. The existence of such a maximum was suggested by Valli et al. (ref 10) who found no improvement in coating adhesion for a titanium interlayer of ∿ 0.3 μm whilst Helmersson et al. reported a beneficial effect for a 0.1 μm titanium interlayer in magnetron sputtered coatings (ref 9). These improvements in adhesion may result from a number of factors which include (i) the dissolution of the weak iron oxide layers at the surface of the component (a chemical gettering effect) or, (ii) the provision of a compliant layer which reduces shear stresses across the coating/substrate interface (a mechanical effect).

SUBSTRATE BIASING DURING DEPOSITION

The application of a substrate bias makes it possible to control the degree of ion-bombardment that the coating experiences during growth, which in turn affects the density, grain size and growth morphology of PVD coatings (refs 2, 4). Fig.4 shows for titanium nitride coatings deposited onto a ferritic tool steel (M2) that the level of compressive internal stress (as determined by the $\sin^2\psi$ X-ray technique) increases with bias voltage due, in the main, to changes in the density of the coating (refs 2, 3). Fracture sections through an unbiased coating show an open columnar structure with each columnar grain, which makes up the coating, a free standing crystal (see fig.5(a)). This type of microstructure can quite readily accommodate any thermal or growth stresses and consequently the stress measured by X-rays is very low in these open-voided

microstructures. In contrast, for a biased titanium nitride coating (fig.5(b)) the individual columns are much less well-defined and by virtue of the denser microstructure substantial stresses can be generated as shown in fig.4. These stresses result in an increase in the elastic strain energy stored in the film which acts at the film/substrate interface and consequently the level of coating adhesion (L_c) decreases with bias voltage (see fig.4). Similar observations of a reduction in critical load with increasing residual stress have been reported for titanium carbide coatings deposited by chemical vapour deposition (ref 11). Also, the presence of a high compressive stress acting in the plane of the coating promotes a denser coating microstructure as reported by Aubert et al. for magnetron sputtered molybdenum coatings (ref 12). In addition, the lattice parameter of titanium nitride coatings increases with internal stress due to the Poisson's ratio effect (ref 3) and is much higher than that of bulk titanium nitride and a number of mechanisms have been proposed to account for this behaviour (ref 4). The internal stress in sputter ion plated coatings can be completely relaxed by dissolution of the substrate, with an accompanying decrease in lattice parameter of the nitride. Therefore it can be concluded that, in these coatings, thermal mismatch stress dominates total stress (see ref 3 for further details).

APPLICATION OF SIP COATINGS

Titanium nitride coatings are being used in a wide variety of applications in order to enhance the performance of components. A good 'rule of thumb' is that TiN coatings will normally appreciably improve the performance of a component that already (uncoated) performs acceptably and finally fails through wear. Badly designed tools, tools that are misused, or tools that fail by fracture rather than wear, are unlikely to benefit from TiN coating. The performance improvement of a coated component depends very greatly on the nature of its application. The characteristics of sputter ion plated TiN coatings which contribute to enhanced performance is their very high hardness (~ 2400 HVN), low coefficient of friction and excellent surface finish; the coating retains the smoothness of the substrate which is extremely important in bearing applications.

Another important consideration is in the improvement in surface finish which occurs through the use of coated tools, and this may give an additional engineering benefit in that a subsequent finishing operation may be omitted. For example, SIP titanium nitride coated drills have demonstrated up to 10 times improvement in life compared with conventional steam tempered drills, with approximately 80% of this improvement in life retained after re-sharpening. But the real benefit lies not in the improved economics from longer tool life but the increased productivity and reduced downtime coupled with the improved quality of holes drilled which means, in some instances, that a subsequent reaming operating may be omitted. Similarly, titanium nitride coated tungsten carbide drawing plugs offer no improvement in life over uncoated plugs, but the improved surface finish on the bore of drawn tubes which results from coating can be an important engineering benefit. The excellent surface finish of SIP TiN coatings makes the coatings particularly attractive for use in anti-seizure coatings and in bearing applications where low frictional properties are desirable. The friction coefficient of TiN running against TiN is extremely low (~ 0.14) and dramatic improvements in bearing life may be realised (in some cases improvements better than x100 have been observed), particularly in abrasive wear situations where stress levels are low. Coupled with low friction, the chemical inertness of TiN has

proved to be very useful in preventing seizure of fasteners used in hot vacuum systems.

In the applications described above, the coating has been deposited onto an existing surface or component and no allowance has been made for the presence of a coating. Fig.6 illustrates how the morphology of chip formation is effected by applying a TiN coating onto thread chasers. Clearly, balling-up of the chip occurs with coated tools, indicating more efficient cutting with less heat generation at the cutting tip, and a chip breaker must be ground in the cutting edge of coated tools to prevent the formation of these potentially dangerous chipballs. This is an example of a more general principle that "tools may have to be redesigned to take full advantage of the engineering benefits of TiN coatings".

CONCLUSIONS

1. SIP is a PVD technique ideally suited to the deposition of hard wear-resistant coatings. To ensure good adhesion of PVD coatings it is necessary to use a number of pre-treatments before deposition of the nitride phase; ion cleaning and the use of titanium interlayers being particularly beneficial in this respect.

2. Titanium nitride coatings can improve the life of many cutting tools but some redesign may be necessary to take full advantage of the engineering benefits of surface coating.

ACKNOWLEDGEMENTS

The authors wish to thank the Department of Trade and Industry for funding and Dr. P.J. Burnett (AERE, Harwell) and Dr. M.H. Jacobs (Ipsen Industries) for their contributions to this work.

REFERENCES

1. A.J. Perry, Surface Eng. 2, 183 (1986).
2. D.S. Rickerby and P.J. Burnett, submitted to Thin Solid Films.
3. D.S. Rickerby, J. Vac. Sci. Technol. A4, 2809 (1986).
4. J.-E. Sundgren, Thin Solid Films 128, 21 (1985).
5. R.A. Dugdale, 'Ion Plating and Applied Techniques' (CEP Consultants, Edinburgh, 1977), p. 177.
6. R.A. Dugdale, Thin Solid Films 45, 541 (1977).
7. D.M. Mattox, J. Vac. Sci. Technol. 10, 47 (1973).
8. J.P. Coad, P. Warrington, R.B. Newbery and M.H. Jacobs, Mater. Des. 6(4), 190 (1985).
9. U. Helmersson, B.O. Johansson, J.-E. Sundgren, H.T.G. Hentzell and P. Billgren, J. Vac. Sci. Technol. A3, 308 (1985).
10. J. Vallí, U. Mäkelä, A. Matthews and V. Murawa, J. Vac. Sci. Technol. A3, 2411 (1985).
11. L. Chollet, H. Boving and H.E. Hintermann, J. Mater. Energy Systems 6, 293 (1985).
12. A. Aubert, J. Danroc, A. Gaucher and J.P. Terrat, Thin Solid Films, 126, 61 (1985).

Fig. 2 Optical micrographs of scratch tracks made on TiN coated stainless steel at a normal load of 15 N. (a) Without a substrate ion clean, (b) with ion cleaning at 900 V

Fig. 5 Scanning electron fractographs (secondary electron image) of (a) unbiased and (b) biased titanium nitride coatings

Fig. 6 Chips from uncoated and coated thread chasers